JEM Journal of Experimental Medicine

ARTICLE

Delineating a serotonin 1B receptor circuit for appetite suppression in mice

Li Li[1], Steven C. Wyler[1], Luis A. León-Mercado[1], Baijie Xu[1], Youjin Oh[4], Swati[1], Xiameng Chen[1], Rong Wan[1], Amanda G. Arnold[1], Lin Jia[5], Guanlin Wang[6], Katherine Nautiyal[7], René Hen[8,9,10], Jong-Woo Sohn[4], and Chen Liu[1,2,3]

Triptans are a class of commonly prescribed antimigraine drugs. Here, we report a previously unrecognized role for them to suppress appetite in mice. In particular, frovatriptan treatment reduces food intake and body weight in diet-induced obese mice. Moreover, the anorectic effect depends on the serotonin (5-HT) 1B receptor (*Htr1b*). By ablating *Htr1b* in four different brain regions, we demonstrate that *Htr1b* engages in spatiotemporally segregated neural pathways to regulate postnatal growth and food intake. Moreover, *Htr1b* in AgRP neurons in the arcuate nucleus of the hypothalamus (ARH) contributes to the hypophagic effects of HTR1B agonists. To further study the anorexigenic Htr1b circuit, we generated *Htr1b-Cre* mice. We find that ARH *Htr1b* neurons bidirectionally regulate food intake in vivo. Furthermore, single-nucleus RNA sequencing analyses revealed that *Htr1b* marks a subset of AgRP neurons. Finally, we used an intersectional approach to specifically target these neurons (Htr1b^{AgRP} neurons). We show that they regulate food intake, in part, through a Htr1b^{AgRP}→PVH circuit.

Introduction

Obesity significantly increases the mortality risk for many diseases, including COVID-19 (Poly et al., 2021). Excessive caloric intake is the primary cause of weight gain. In support of this notion, many obesity-linked genes are present in the brain and have been shown to regulate satiety (O'Rahilly, 2009). With the help of new optogenetic, chemogenetic, and neuroimaging tools, recent studies have uncovered a series of neural circuits that control food intake (Moran and Ladenheim, 2016). However, despite these advances, druggable targets with well-illustrated mechanisms for appetite control remain scarce. In this regard, the central serotonin (5-HT) system has been a target for multiple weight-loss medications since the 1960s. Compounds that elevate brain 5-HT content reduce food intake and body weight (Wyler et al., 2017). The therapeutic potential of this pathway was highlighted by the observation that the anorectic effect of d-fenfluramine, the active ingredient of the once-popular diet pill fenfluramine/phentermine, was mediated, in part, through the activation of 5-HT 2C receptors (*Htr2c*; Heisler et al., 2002; Tecott et al., 1995). Subsequently, lorcaserin (Belviq), an Htr2c-specific agonist, became the first novel anti-obesity medication in 1997 (Colman et al., 2012). Unfortunately, lorcaserin was recently removed from the market due to unexpected cancer risk (Sharretts et al., 2020), casting doubt on the future use of other Htr2c agonists as anti-obesity therapies.

Observations in humans and mice showed that the anorectic effect of lorcaserin is less potent than that of d-fenfluramine or other serotonergic agents (Berglund et al., 2013; Colman et al., 2012). These findings, therefore, suggest the involvement of additional 5-HT receptors behind the hypophagic effect. In search of new 5-HT–based weight-loss therapies, we found that agonists for 5-HT 1B receptor (*Htr1b*) dose-dependently reduced food intake in C57BL/6 mice. These include several triptans, a class of commonly used antimigraine drugs that manifest few health risks after long-term use (Ghanshani et al., 2020; Robbins, 2004). Notably, the anorectic effect of Htr1b-specific agonists appeared to be more potent than that of lorcaserin, the specific agonist for Htr2c. Furthermore, such an effect was independent of *Htr2c* but required endogenous *Htr1b*. Using a

[1]The Hypothalamic Research Center, Department of Internal Medicine, UT Southwestern Medical Center, Dallas, TX; [2]Department of Neuroscience, UT Southwestern Medical Center, Dallas, TX; [3]Peter O'Donnell Jr. Brain Institute, UT Southwestern Medical Center, Dallas, TX; [4]Department of Biological Sciences, Korea Advanced Institute of Science and Technology, Daejeon, Korea; [5]Department of Biological Sciences, The University of Texas at Dallas, Richardson, TX; [6]Centre for Computational Biology, Medical Research Council Weatherall Institute of Molecular Medicine, University of Oxford, Oxford, UK; [7]Department of Psychological and Brain Sciences, Dartmouth College, Hanover, NH; [8]Department of Psychiatry, Columbia University and Research Foundation for Mental Hygiene, New York State Psychiatric Institute, New York, NY; [9]Department of Neuroscience, Columbia University, New York, NY; [10]Department of Pharmacology, Columbia University, New York, NY.

Correspondence to Chen Liu: chen.liu@utsouthwestern.edu; Jong-Woo Sohn: jwsohn@kaist.ac.kr

Guanlin Wang's current address is Shanghai Key Laboratory of Metabolic Remodeling and Health, Institute of Metabolism and Integrative Biology, Fudan University, Shanghai, China.

combination of genetic, transcriptomic, and behavioral analyses, we have investigated the underlying neural pathways behind the pharmacological and physiological effects of *Htr1b* activation on food intake and body weight. Collectively, our findings suggest that *Htr1b* is a new target for 5-HT–based weight-loss therapies.

Results

The anorectic effect of triptans depends on *Htr1b*

Triptans are a class of antimigraine drugs that display partial Htr1b agonistic activity (Martin et al., 1997; Wang et al., 2013). We investigated whether these drugs may also possess anorexigenic properties. To this end, we surveyed six commonly prescribed triptans by administering an intraperitoneal (IP) dose of either triptan or vehicle (saline) to C57BL/6J mice after an 18-h fast and measuring subsequent food intake. We found that four of the six triptans significantly suppressed fasting-induced hunger (Fig. 1 A). Among them, frovatriptan manifested the strongest effect. Importantly, we found that the hypophagic effect of frovatriptan was dependent upon endogenous *Htr1b* and was absent in mice lacking these receptors ($Htr1b^{null/null}$ mice; Fig. 1 B; Saudou et al., 1994).

We next evaluated the anti-obesity effect of frovatriptan in diet-induced obese mice (Fig. 1 C). Briefly, male C57BL/6J mice were fed a high-fat diet (HFD, 60 kcal% fat, D12492i Research Diets) for 7 wk. Obese mice (>40 g) with comparable weights were then segregated into two groups and treated with either frovatriptan or vehicle while still being fed HFD. A daily IP dose of frovatriptan (10 mg/kg) reduced body weight in HFD-fed mice by 3.58 ± 1.61% within 24 d (Fig. 1 D). In contrast, vehicle-treated controls gained 5.83 ± 2.04% weight during the same period. Consistent with this finding, frovatriptan-treated mice had decreased food intake compared to vehicle-treated controls (Fig. 1 E). In another paradigm, chronic (14-d) infusion of frovatriptan (7 mg/kg/d) via implanted osmotic minipumps yielded a similar weight loss (−2.3 ± 1.75% vs. +5.1 ± 1.65% in controls). Furthermore, nuclear magnetic resonance analyses revealed that frovatriptan infusion reduced fat mass, but not lean mass, after the 14-d treatment (Fig. 1 F). Fat loss was evident in both inguinal and epididymal white adipose tissues. In contrast, the weight of brown adipose tissue remained constant between frovatriptan- and vehicle-treated mice (Fig. 1 G). Concomitant with the weight loss was an improvement in glucose homeostasis, as frovatriptan-treated mice exhibited accelerated glucose clearance in a glucose tolerance test (GTT; Fig. 1 H).

The anorexigenic effect of Htr1b agonist is independent of *Htr2c*

To study the mechanism behind the anorectic effect, we used CP94253, a selective Htr1b agonist (Halford and Blundell, 1996). We found that CP94253 dose-dependently inhibited fasting-induced refeeding in wild-type mice (Fig. 2 A). As predicted, the hypophagic effect was blunted in $Htr1b^{null/null}$ mice (Fig. 2 B). Notably, we found that the anorectic effect of CP94253 appeared to be more potent than that of lorcaserin, the anti-obesity drug targeting Htr2c. It suppressed refeeding at a lower dose (2.5 vs. 10 mg/kg) and for a longer period (90 vs. 30 min) in the same test (Fig. S1).

Expressions of *Htr1b* and *Htr2c* are enriched in the hypothalamus, a critical regulator of food intake. Furthermore, infusion of m-chloro-phenylpiperazine, a partial agonist for both Htr1b and Htr2c in the hypothalamus, inhibits food intake in rats (Hikiji et al., 2004). However, it is unclear whether these two receptors act on a common neural pathway to regulate satiety. Moreover, a recent study suggested that the hypophagic effect of Htr1b agonists may require co-activation of Htr2c receptors (Doslikova et al., 2013). We investigated this hypothesis by first examining the anorectic effect of the Htr1b agonist, CP94253, in *Htr2c* null mice (Xu et al., 2008). We found that CP94253 suppressed fasting-induced refeeding in these mice as it did in wild-type controls (Fig. 2 C), suggesting that its anorexigenic effect does not require *Htr2c*. In support of this finding, *Htr2c* null mice had normal levels of *Htr1b* mRNA in the hypothalamus (Fig. 2 D). On the other hand, lorcaserin, a specific agonist for Htr2c, inhibited refeeding in $Htr1b^{null/null}$ mice (Fig. 2 E). Likewise, loss of *Htr1b* had no effect on the hypothalamic expression of *Htr2c* or other appetite regulators, such as *Pomc*, *Npy*, or *Agrp* (Fig. 2 F). Finally, it was previously shown that *Htr2c* acts on proopiomelanocortin (POMC) neurons to suppress food intake and that such anorectic actions require melanocortin 4 receptors (*Mc4r*) in downstream *Sim1* neurons (Berglund et al., 2013; Xu et al., 2008; Xu et al., 2010). In contrast, we found that these receptors were dispensable for the hypophagic effect of CP94253, as refeeding was still inhibited in $Mc4r^{Sim1\text{-}KO}$ mice lacking *Mc4r* in *Sim1-Cre* expressing neurons (Fig. 2 G; Li et al., 2021a). Together, these findings suggest that *Htr1b* and *Htr2c* act on different neural pathways to regulate food intake.

Htr1b engages distinct neural pathways to regulate postnatal growth and appetite

Given the anorexigenic effect of Htr1b agonists, is *Htr1b* necessary for normal food intake and body weight homeostasis? A recent phenotypic screen for developmental deficits in all available C57BL/6 knockout mice identified *Htr1b* as one of the "sub-viable" genes with partial perinatal lethality (Dickinson et al., 2016). Consistent with these results, we found that C57BL/6 $Htr1b^{null/null}$ mice weighed less than both wild-type and heterozygous $Htr1b^{null/+}$ littermates at the time of weaning (Fig. 3 A). Despite a modest weight reduction, chow diet–fed $Htr1b^{null/null}$ mice had otherwise comparable growth curves to their littermate controls (Fig. 3 B). Furthermore, body weight did not diverge when weight-matched control and $Htr1b^{null/null}$ mice were challenged with an HFD (60 kcal% fat) for 6 wk (Fig. 3 C). Moreover, indirect calorimetry analyses found no difference in food intake, oxygen consumption, respiratory exchange ratio, or physical activity (Fig. 3, D–G) between weight-matched controls and $Htr1b^{null/null}$ mice. These findings indicate that adult $Htr1b^{null/null}$ mice have normal energy intake and expenditure despite a developmental delay in growth.

We next investigated the brain regions where Htr1b agonists might act to promote satiety. Notably, unlike *Htr2c*, *Htr1b* is expressed on both 5-HT and non–5-HT neurons. *Htr1b* could act on postsynaptic neurons (heteroreceptors) to regulate food

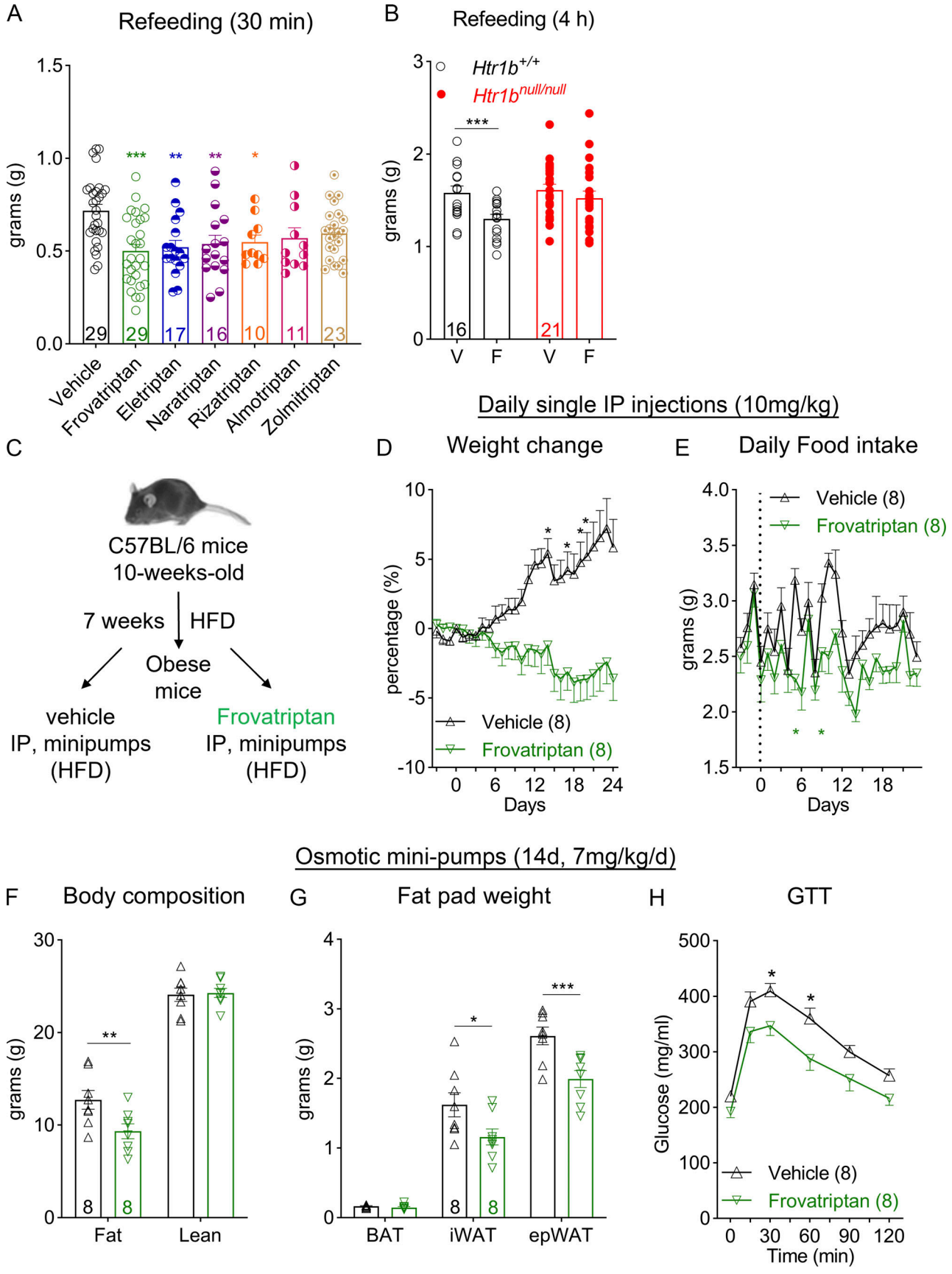

Figure 1. **The anti-obesity effect of triptans. (A)** Refeeding in mice treated with vehicle or triptans (10 mg/kg) after an overnight (18 h) fast, n = 10–29 per group, F (6, 127) = 4.741, one-way ANOVA, P < 0.001. **(B and C)** Refeeding in *Htr1b*$^{+/+}$ and *Htr1b*$^{null/null}$ mice treated with vehicle (V) or frovatriptan (F; 10 mg/kg)

after an overnight fast, n = 16–21 per genotype, F (1, 35) = 4.89, P = 0.034. **(C)** Schematic for the experiments evaluating the anti-obesity effect of frovatriptan in diet-induced obese mice. **(D)** Change in body weight, n = 8, F (27, 378) = 14.63, P < 0.0001. **(E)** Daily food intake, n = 8, F (26, 364) = 2.023, P = 0.0026. **(F)** Body composition, n = 8, F (1, 14) = 7.064, P = 0.0187. **(G)** Fat pad weight, n = 8, F (2, 42) = 3.914, P = 0.028. **(H)** GTT after the 14-d treatment with vehicle or frovatriptan, n = 8, F (1, 14) = 7.765, P = 0.015. Data are presented as mean ± SEM. Two-way ANOVA with Sidak's post hoc tests in B and D–H. *, P < 0.05; **, P < 0.01; and ***, P < 0.001. All data were verified in at least two independent experiments. BAT, brown adipose tissue; epWAT, epididymal white adipose tissue; iWAT, inguinal white adipose tissue.

intake. Alternatively, it may influence feeding by regulating 5-HT release on 5-HT neurons (autoreceptors; Stamford et al., 2000). To evaluate the impact of autoreceptor vs. heteroreceptor function on food intake, we selectively ablated *Htr1b* in either 5-HT neurons (*Htr1b*$^{Pet1\text{-}KO}$, autoreceptor knockout; Fig. 4, A–D) or the hypothalamus (*Htr1b*$^{Foxd1\text{-}KO}$, hypothalamic heteroreceptor knockout; Fig. 4, E–H). Of note, *Pet1-Cre* activity in the brain is restricted to 5-HT neurons (Liu et al., 2010; Scott et al., 2005), whereas *Foxd1-Cre* specifically targets progenitors that give rise to neurons in the hypothalamus and prethalamus (Salvatierra et al., 2014). In situ hybridization and quantitative PCR (qPCR) in *Htr1b*$^{Pet1\text{-}KO}$ mice showed that *Htr1b* mRNA was depleted in the dorsal raphe where cell bodies of 5-HT neurons reside (Fig. S2, A and B). However, hypothalamic expression remained intact (Fig. S2 C). In contrast, similar analyses in *Htr1b*$^{Foxd1\text{-}KO}$ mice detected normal levels of *Htr1b* mRNA in the dorsal raphe and loss of expression in the hypothalamus (Fig. S2, D–F).

Remarkably, deleting *Htr1b* in 5-HT neurons was sufficient to reproduce the growth deficit seen in *Htr1b*$^{null/null}$ mice. *Htr1b*$^{Pet1\text{-}KO}$ mice had a similar weight decrease at weaning (Fig. 4 B) that persisted into adulthood (Fig. 4 C). As predicted, *Htr1b*$^{Pet1\text{-}KO}$ mice had normal energy intake and expenditure compared to weight-matched controls (*Htr1b*$^{fl/fl}$; Fig. S2, H–K). However, unlike *Htr1b*$^{null/null}$ mice, the anorectic response to CP94253 was preserved in these mice (Fig. 4 D), suggesting that *Htr1b* autoreceptors are dispensable for this behavior. In contrast, *Htr1b*$^{Foxd1\text{-}KO}$ mice had normal body weights at weaning and in adulthood (Fig. 4, F and G). In addition, neither CP94253 nor frovatriptan suppressed fasting-induced refeeding in these mice (Fig. 4 H and Fig. S2 G), indicating that *Htr1b* in these neurons is necessary for the anorectic effect. Collectively, these results support the notion that *Htr1b* acts on divergent neural pathways to regulate feeding and postnatal growth.

Within the hypothalamus, *Htr1b* expression has been reported in ARH AgRP neurons (Heisler et al., 2006) and neurons in the paraventricular nucleus (PVH; Hutson et al., 1988). However, their physiological roles in these neurons have not been investigated. To further isolate the neurons that mediate the anorexigenic effect of Htr1b agonists, we generated *Htr1b*$^{Agrp\text{-}KO}$ mice, in which *Htr1b* was selectively deleted from *Agrp-Cre* neurons (Tong et al., 2008) and *Htr1b*$^{Sim1\text{-}KO}$ mice, in which *Htr1b* was selectively deleted from PVH neurons expressing *Sim1-Cre* (Balthasar et al., 2005; Fig. 4 I). In situ hybridization (RNAscope) experiments detected *Htr1b* mRNA in a subset of *Sim1-Cre* and *Agrp-Cre* neurons in control mice (*Htr1b*$^{fl/fl}$). In contrast, *Htr1b* mRNA was absent in these neurons in *Htr1b*$^{Sim1\text{-}KO}$ and *Htr1b*$^{Agrp\text{-}KO}$ mice (Fig. 4, J and L). Moreover, both conditional knockouts had normal body weights at weaning and in adulthood (Fig. S3, A–D). Intriguingly, we found that CP94253 inhibited fasting-induced refeeding in *Htr1b*$^{Sim1\text{-}KO}$ but not in *Htr1b*$^{Agrp\text{-}KO}$ mice (Fig. 4, K and M). Consistent with this finding, the anorectic effect of frovatriptan was blunted in *Htr1b*$^{Agrp\text{-}KO}$ mice (Fig. S3 E). Therefore, these findings identify *Agrp* neurons as one site where Htr1b agonists act to suppress food intake.

Htr1b^{ARH} neurons bidirectionally regulate food intake in vivo

To probe the neural basis of the anorexigenic *Htr1b* circuit further, we generated *Htr1b-Cre* mice (*Htr1b*$^{P2A\text{-}iCre}$) for which the expression of a codon-improved Cre recombinase (*iCre*; Shimshek et al., 2002) is governed by endogenous regulatory sequences of the *Htr1b* gene (Fig. 5 A). Furthermore, the coding sequences of *Htr1b* and *iCre* are linked by a peptide bridge P2A sequence (Tang et al., 2016) so that *iCre* is transcribed in the same neurons and at the same levels as the endogenous *Htr1b*. PCR genotyping verified the insertion of *iCre* into the endogenous *Htr1b* locus (Fig. 5 B). *Htr1b* is highly expressed in cerebellar Purkinje cells in the mouse brain (Lein et al., 2007), which we corroborated using riboprobes (RNAscope) against *Htr1b* transcripts. Moreover, we found that mRNA for *Htr1b* and *iCre*, as well as proteins for a Cre-activated nuclear tdTomato reporter (*Ai75*) were co-expressed in the same neurons (Fig. 5 C).

With this new mouse model, we observed *Htr1b* mRNA along with the Cre-activated tdTomato reporter in the ARH (Fig. 5, D–F). Thus, we designated ARH neurons expressing *Htr1b* as Htr1b^{ARH} neurons. Combined in situ hybridization (RNAscope) and immunofluorescence analyses showed that *Htr1b* was expressed by both AgRP and non-AgRP neurons (Fig. 5 E). However, Htr1b^{ARH} neurons did not express *Pomc* (Fig. 5 F). Moreover, we found that some Htr1b^{ARH} neurons were activated by fasting as evidenced by increased Fos protein (Fig. 5, G and H), a marker for elevated neuronal activity.

To test whether Htr1b^{ARH} neurons directly regulate food intake, we stereotaxically delivered adeno-associated viruses (AAVs) expressing Cre-dependent Designer Receptors Exclusively Activated by Designer Drugs (DREADD) constructs (Roth, 2016) into the ARH of *Htr1b-Cre* mice (Fig. 5 I). In *Htr1b-Cre* mice that received bilateral injections of the stimulatory DREADD (hM3Dq), bath application of compound 21 (C21; 5 µM), a selective DREADD agonist (Thompson et al., 2018), depolarized Htr1b^{ARH} neurons by 6.3 ± 0.4 mV (Fig. 5 J; from −44.3 ± 0.8 to −38.0 ± 0.4 mV; n = 4). The action potential (AP) frequency was increased from 0.8 ± 0.4 to 2.9 ± 1.3 Hz (n = 4). Moreover, we found that an IP dose of C21 (1 mg/kg) acutely boosted food consumption in satiated mice (Fig. 5 K). In comparison, C21 did not increase food intake in mice that received viruses containing a control construct (mCherry). Furthermore, chronic C21 treatment (IP, 1 mg/kg once a day) resulted in a sustained increase in food intake in these mice (Fig. 5 L). To evaluate the impact of

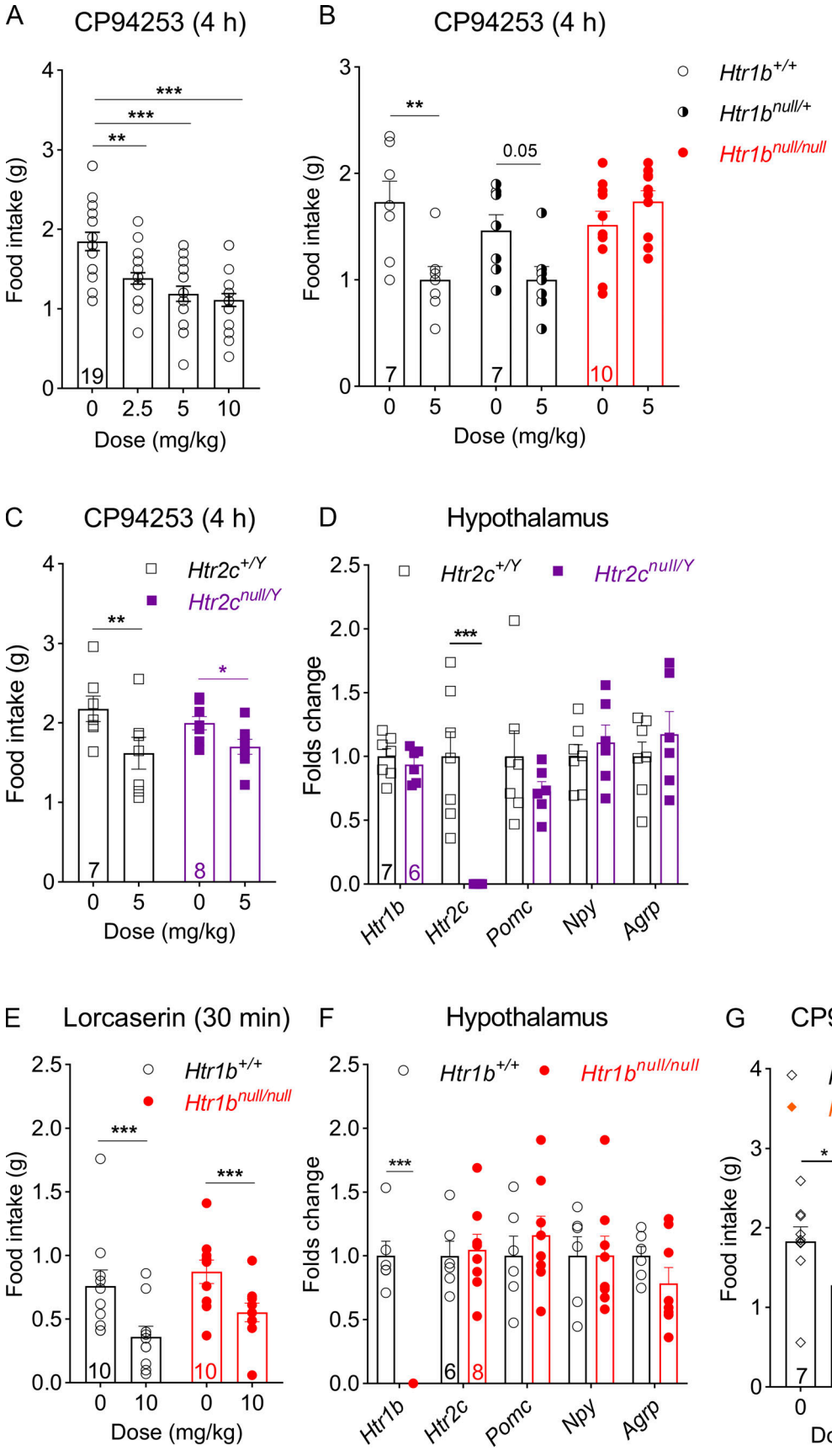

Figure 2. ***Htr1b* and *Htr2c* independently regulate food intake. (A)** Refeeding in mice treated with CP94253 after an overnight (18 h) fast, *n* = 19 per group, F (3, 72) = 12.68, one-way ANOVA, P < 0.001. **(B)** The anorectic effect of CP94253 in *Htr1b*$^{+/+}$, *Htr1b*$^{null/+}$, and *Htr1b*$^{null/null}$ mice, *n* = 7–10 per genotype, F (2, 21) =

8.923, P = 0.0016. **(C)** The anorectic effect of CP94253 in *Htr2c*$^{+/Y}$ and *Htr2c*$^{null/Y}$ mice, *n* = 7–8, F (1, 13) = 24.97, P < 0.001. **(D)** qPCR analysis of hypothalamic mRNAs in *Htr2c*$^{+/Y}$ and *Htr2c*$^{null/Y}$ mice, *n* = 6–7, unpaired *t* test. **(E)** The anorectic effect of lorcaserin in *Htr1b*$^{+/+}$ and *Htr1b*$^{null/null}$ mice, *n* = 10, F (1, 18) = 46.76, P < 0.001. **(F)** qPCR analysis of hypothalamic mRNAs in *Htr1b*$^{+/+}$ and *Htr1b*$^{null/null}$ mice, *n* = 6–8, unpaired *t* test. **(G)** The anorectic effect of CP94253 in *Mc4r*$^{fl/fl}$ and *Mc4r*$^{Sim1\text{-}KO}$ mice, *n* = 7–9, F (1, 14) = 27.57, P < 0.001. Data are presented as mean ± SEM. Two-way ANOVA with Sidak's post hoc tests in B, C, E, and G. *, P < 0.05; **, P < 0.01; and ***, P < 0.001. All data were verified in at least two independent experiments.

inhibiting Htr1b^{ARH} neurons on food intake, we bilaterally injected AAVs containing the inhibitory DREADD (hM4Di). Whole-cell electrophysiological recordings showed that C21 hyperpolarized Htr1b^{ARH} neurons by −16.0 ± 1.8 mV (Fig. 5 M; from −45.8 ± 1.3 to −61.8 ± 0.6 mV; *n* = 4). The AP frequency was decreased from 0.5 ± 0.2 to 0.0 ± 0.0 Hz (*n* = 4). In addition, adult silencing of these neurons with C21 (IP, 1 mg/kg) inhibited fasting-induced refeeding and daily food intake (Fig. 5, N and O). Taken together, these findings demonstrate that *Htr1b*^{ARH} neurons can bidirectionally regulate food intake in vivo.

Htr1b marks a subset of *Agrp* neurons

AgRP neurons integrate metabolic cues through multiple hormones such as leptin, ghrelin, and 5-HT (Heisler et al., 2006; Wang et al., 2014; Xu et al., 2018). Our histological analyses demonstrated that *Htr1b* expression marks a subset of AgRP neurons. We surveyed the adult ARH along the rostral–caudal

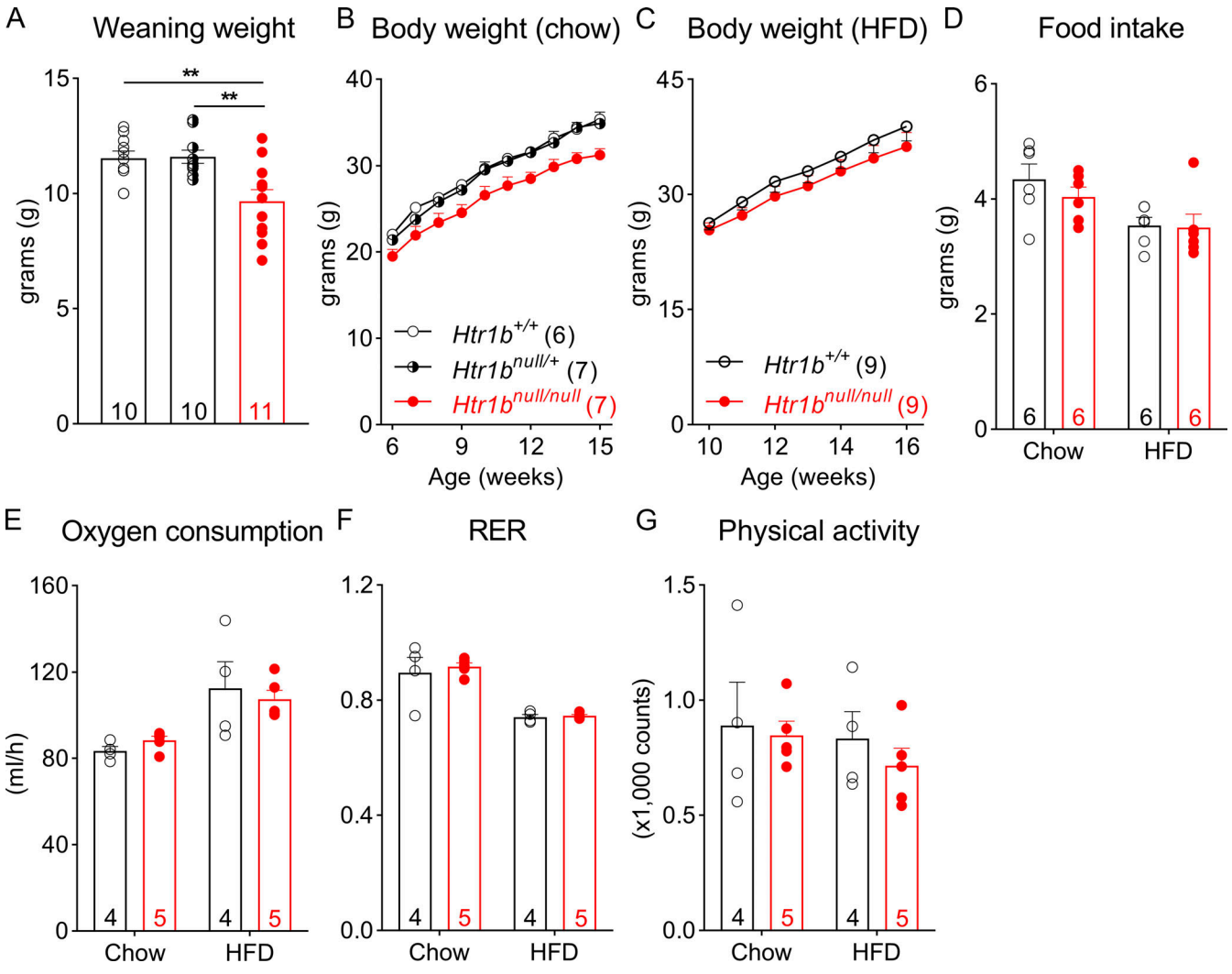

Figure 3. **Developmental growth delay but normal energy intake and expenditure in adult *Htr1b*$^{null/null}$ mice. (A)** Body weight at 3 wk of age, *n* = 10–11, F (2, 28) = 8.024, one-way ANOVA, P = 0.0018, **, P < 0.01. **(B)** Body weight curves in chow-fed mice, *n* = 6–7, F (18, 153) = 1.214, P = 0.26. **(C)** Body weight curves in weight-matched *Htr1b*$^{+/+}$ and *Htr1b*$^{null/null}$ mice fed a HFD for 6 wk, *n* = 9, F (6, 96) = 0.604, P = 0.73. **(D)** Daily food intake in weight-matched *Htr1b*$^{+/+}$ and *Htr1b*$^{null/null}$ mice fed a chow diet or HFD, *n* = 6, F (1, 10) = 1.084, P = 0.32. **(E)** Oxygen consumption in weight-matched *Htr1b*$^{+/+}$ and *Htr1b*$^{null/null}$ mice fed a chow diet or HFD, *n* = 4–5, F (1, 7) = 0.7788, P = 0.41. **(F)** Respiratory exchange ratio (RER) in weight-matched *Htr1b*$^{+/+}$ and *Htr1b*$^{null/null}$ mice fed a chow diet or HFD, *n* = 4–5, F (1, 7) = 0.094, P = 0.77. **(G)** Physical activity in weight-matched *Htr1b*$^{+/+}$ and *Htr1b*$^{null/null}$ mice fed a chow diet or HFD, *n* = 4–5, F (1, 7) = 0.2521, P = 0.63. Data are presented as mean ± SEM. Two-way ANOVA with Sidak's post hoc tests in B–G. All data were verified in at least two independent experiments.

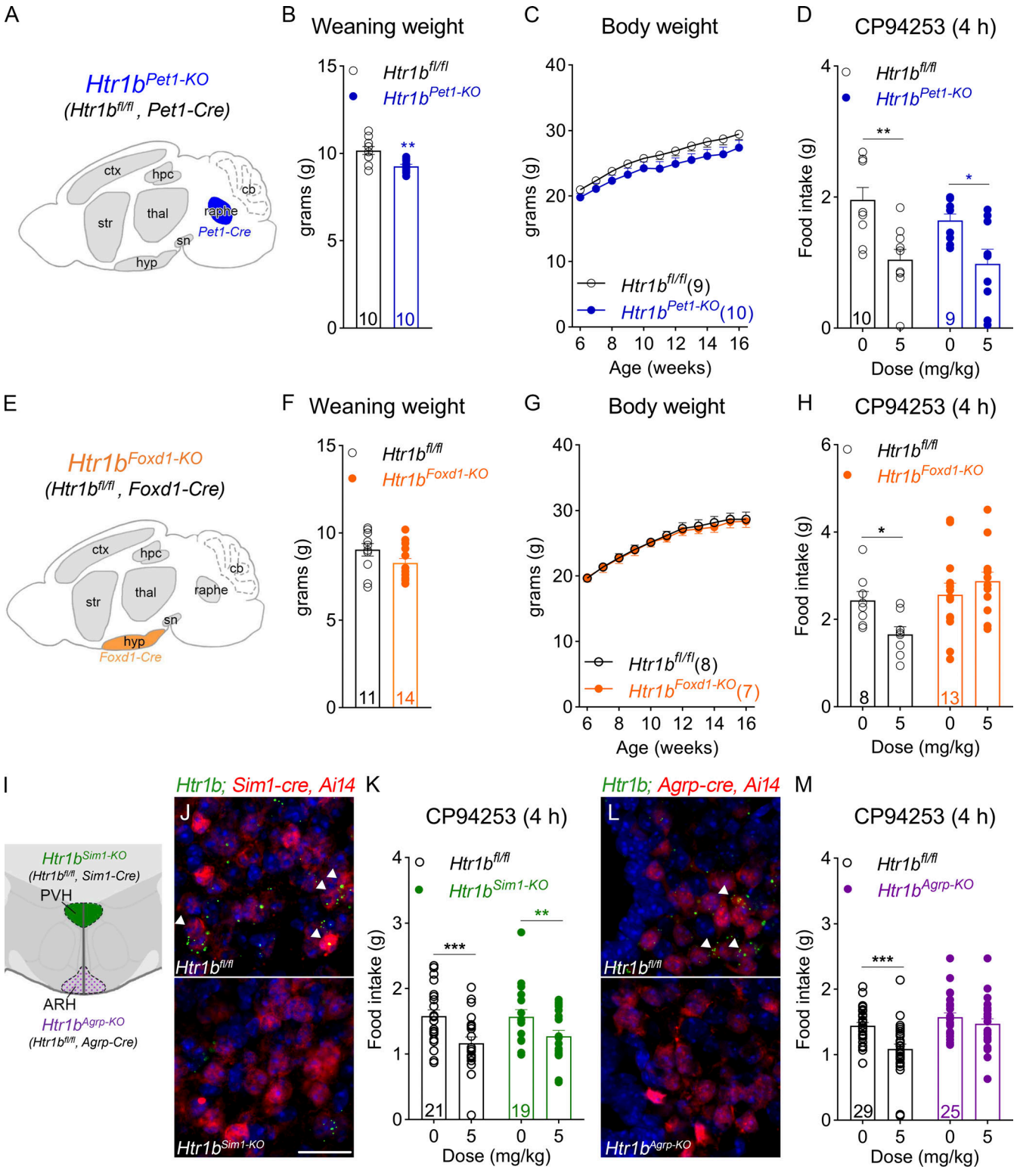

Figure 4. **Activation of *Htr1b* in *AgRP* neurons suppresses food intake. (A)** Schematic for deleting *Htr1b* in *Pet1-Cre* neurons, the autoreceptor knockout $Htr1b^{Pet1\text{-}KO}$ mice. *Pet1-Cre* expression in the brain is restricted to 5-HT neurons. **(B)** Body weight at 3 wk of age, n = 10, unpaired t test, P = 0.002. **(C)** Body weight curves in chow-fed $Htr1b^{fl/fl}$ and $Htr1b^{Pet1\text{-}KO}$ mice, n = 9–10, F (10, 170) = 1.298, P = 0.24. **(D)** The anorectic effect of CP94253 in $Htr1b^{fl/fl}$ and $Htr1b^{Pet1\text{-}KO}$ mice, n = 9–10, F (1, 17) = 22.6, P < 0.001. **(E)** Schematic for deleting *Htr1b* in *Foxd1-Cre* neurons, the hypothalamic heteroreceptor knockout $Htr1b^{Foxd1\text{-}KO}$ mice. *Foxd1-Cre is* developmentally expressed in the progenitor cells that generate hypothalamic neurons. **(F)** Body weight at 3 wk of age, n = 11–14, unpaired t test, P = 0.12. **(G)** Body weight curves in chow-fed $Htr1b^{fl/fl}$ and $Htr1b^{Foxd1\text{-}KO}$ mice, n = 7–8, F (10, 130) = 0.292, P = 0.98. **(H)** The anorectic effect of CP94253 in $Htr1b^{fl/fl}$ and $Htr1b^{Foxd1\text{-}KO}$ mice, n = 8–13, F (1, 19) = 7.945, P = 0.011. **(I)** Schematic for deleting *Htr1b* in hypothalamic *Sim1-Cre* and *Agrp-Cre* neurons. *Sim1-Cre* expression is enriched in the PVH. *Agrp-Cre* expression is restricted to the ARH. **(J)** Fluorescence for *Htr1b* mRNAs (RNAscope, green) and *Sim1-Cre* activated

tomato reporter (red). **(K)** The anorectic effect of CP94253 in *Htr1b*$^{fl/fl}$ and *Htr1b*$^{Sim1\text{-}KO}$ mice, n = 19–21, F (1, 38) = 30.07, P < 0.001. **(L)** Fluorescence for *Htr1b* mRNAs (RNAscope, green) and *Agrp-Cre* activated tomato reporter (red). **(M)** The anorectic effect of CP94253 in *Htr1b*$^{fl/fl}$ and *Htr1b*$^{Agrp\text{-}KO}$ mice, n = 25–29, F (1, 52) = 23.1, P < 0.001. Data are presented as mean ± SEM. Two-way ANOVA with Sidak's post hoc tests in C and D, G and H, K, and M. *, P < 0.05; **, P < 0.01; and ***, P < 0.001. Scale bars in J and L are 20 µm. All data were verified in at least two independent experiments.

axis and found that 14.81 ± 1.68% of *Npy* positive neurons (another marker for AgRP neurons) expressed mRNA for *Htr1b* (n = 3 mice; Fig. 6 A). To shed light on this subpopulation of AgRP neurons, we carried out single-nucleus RNA sequencing (snRNA-seq) in the ARH of *AgRP-Cre; Sun1-GFP* mice. We used FACS to enrich GFP-positive nuclei from 15 adult mice (Fig. S4 A). Nuclei from individual mice were tagged with unique DNA barcodes (Gaublomme et al., 2019) before being pooled for library preparation and subsequent sequencing (Fig. S4, B and C). As has been shown previously (Yu et al., 2021), although the additional FACS step did not completely eliminate other cell types, it allowed us to harvest a higher percentage of AgRP neurons for subsequent analyses. After demultiplexing and quality control steps, we used uniform manifold approximation and projection (UMAP) and Louvain clustering analyses (Becht et al., 2018) to isolate neuronal and non-neuronal cell clusters (Fig. S4, D–F). We identified 4,882 nuclei from neurons, among which, 2,742 contained reads (unique molecular identifier [UMI] ≥ 1) for either *Agrp* or *Npy*. UMAP and clustering analyses on these neurons further revealed four clusters with distinct transcriptomic profiles. Notably, 89% of the AgRP neurons (2,433 out of 2,742) form the two biggest cell clusters (Fig. 6 B). Between them, we found that *Agrp* expression was significantly higher in one cluster than in the other (Fig. 6 C). In comparison, *Npy* levels were comparable between the two groups (Fig. 6 D). We, therefore, named the two subpopulations as AgRP^{High} and AgRP^{Low}, respectively. Consistent with our histological data, snRNA-seq analyses detected *Htr1b* expression in a subset of AgRP neurons (Fig. 6 E). Interestingly, we found that *Htr1b* was enriched in the AgRP^{Low} subset, whereas the leptin receptor (*Lepr*) was predominantly expressed by neurons in the AgRP^{High} subgroup (Fig. 6 F). Few AgRP neurons (8 out of 2,742) expressed both transcripts. In support of this finding, pSTAT3, a reporter of leptin signaling, was induced in only a small percentage of ARH *Htr1b-Cre* neurons (16.6 ± 2.05%, n = 3 mice; Fig. 6 G) after an IP dose of leptin (3 mg/kg).

Htr1b^{AgRP} neurons regulate food intake through a Htr1b$^{AgRP→PVH}$ circuit

To study the *Htr1b*-expressing AgRP neurons (designated hereafter as Htr1b^{AgRP} neurons), we adopted an intersectional targeting approach using double transgenic mice (*Htr1b*$^{Cre/+}$; *Npy*$^{Flp/+}$) expressing both *Htr1b-Cre* and *Npy-Flp*. We stereotaxically delivered AAV viruses containing a Cre- and Flp-dependent EYFP reporter in the ARH of these mice. Reporter expression was dependent upon the activities of both Cre and Flp recombinases so that EYFP was expressed only in Htr1b^{AgRP} neurons. 3 wk after AAV injection, we detected EYFP fluorescence in a small number of neurons in the ARH. Of note, EYFP signals were absent in other hypothalamic neurons that expressed *Htr1b-Cre* (e.g., those in the PVH; Fig. S5 A). Furthermore, EYFP was absent in wild-type, *Htr1b*$^{Cre/+}$, or *Npy*$^{Flp/+}$ mice that received the same viruses (Fig. S5 B). Anatomically, we found that the EYFP-labeled neurons were clustered in the mediobasal part of the ARH, adjacent to the third ventricle (Fig. 7 A). The distribution of cell bodies was similar to that of Htr1b-Cre; Sun1-GFP positive neurons in the same area, where *Htr1b* mRNA was enriched (Figs. 5, D and G; and 7 A). To determine whether Htr1b^{AgRP} neurons could directly regulate food intake in vivo, we utilized AAV constructs that expressed Cre- and Flp-dependent channelrhodopsin2-EYFP (ChR2-EYFP) fusion proteins (Fenno et al., 2014). In *Htr1b*$^{Cre/+}$; *Npy*$^{Flp/+}$ mice that received injections of ChR2-EYFP AAVs, optical stimulation of the ARH induced c-Fos protein expression in EYFP positive neurons (Fig. 7 B). Moreover, unilateral activation of these neurons increased food intake in satiated mice (Fig. 7, C and D). It has been reported that stimulation of AgRP neurons boosts food intake through parallel and redundant downstream projections to the PVH, lateral hypothalamic area (LHA), paraventricular thalamic nucleus (PVT), and anterior subdivisions of the bed nucleus of the stria terminalis (aBNST; Betley et al., 2013). Therefore, we investigated whether Htr1b^{AgRP} neurons innervated these areas. We did not observe EYFP-positive neurites in the LHA or aBNST (Fig. 7 E). In comparison, we found the majority of EYFP-labeled axons in the PVH, but few in the PVT. Finally, to test the functional relevance of Htr1b^{AgRP} neuron projections on food intake, we optogenetically stimulated the Htr1b^{AgRP} neuron axons in the abovementioned four targets. We found that terminal stimulation in the PVH produced a similar increase in food intake (0.37 ± 0.03 g) to that of cell body stimulation (0.43 ± 0.03 g; Fig. 7, F and G), whereas comparable manipulations in the PVT, LHA, or aBNST had no effect on food intake, thereby confirming the critical role of PVH neurons in this circuit.

Discussion

The central 5-HT system is a critical regulator of satiety and has been a key target for weight-loss therapies. However, globally augmenting 5-HT signaling can lead to adverse and sometimes fatal consequences. For example, d-fenfluramine was banned after reports of valvular heart disease and pulmonary hypertension in users (Connolly et al., 1997). To minimize side effects, focus has shifted to identifying 5-HT receptor pathways that specifically mediate the anorectic actions of 5-HT.

Although there are 15 serotonin receptor subtypes, only agonists for the *Htr2c* or *Htr1b* reduce food intake (Bovetto and Richard, 1995). Moreover, the appetite suppressing effect of d-fenfluramine is blunted in mice lacking either of these receptors (Lucas et al., 1998; Tecott et al., 1995). Since these initial discoveries, more than a decade of work has demonstrated that the activation of *Htr2c* on hypothalamic and brainstem POMC neurons suppresses appetite (Berglund et al., 2013; D'Agostino

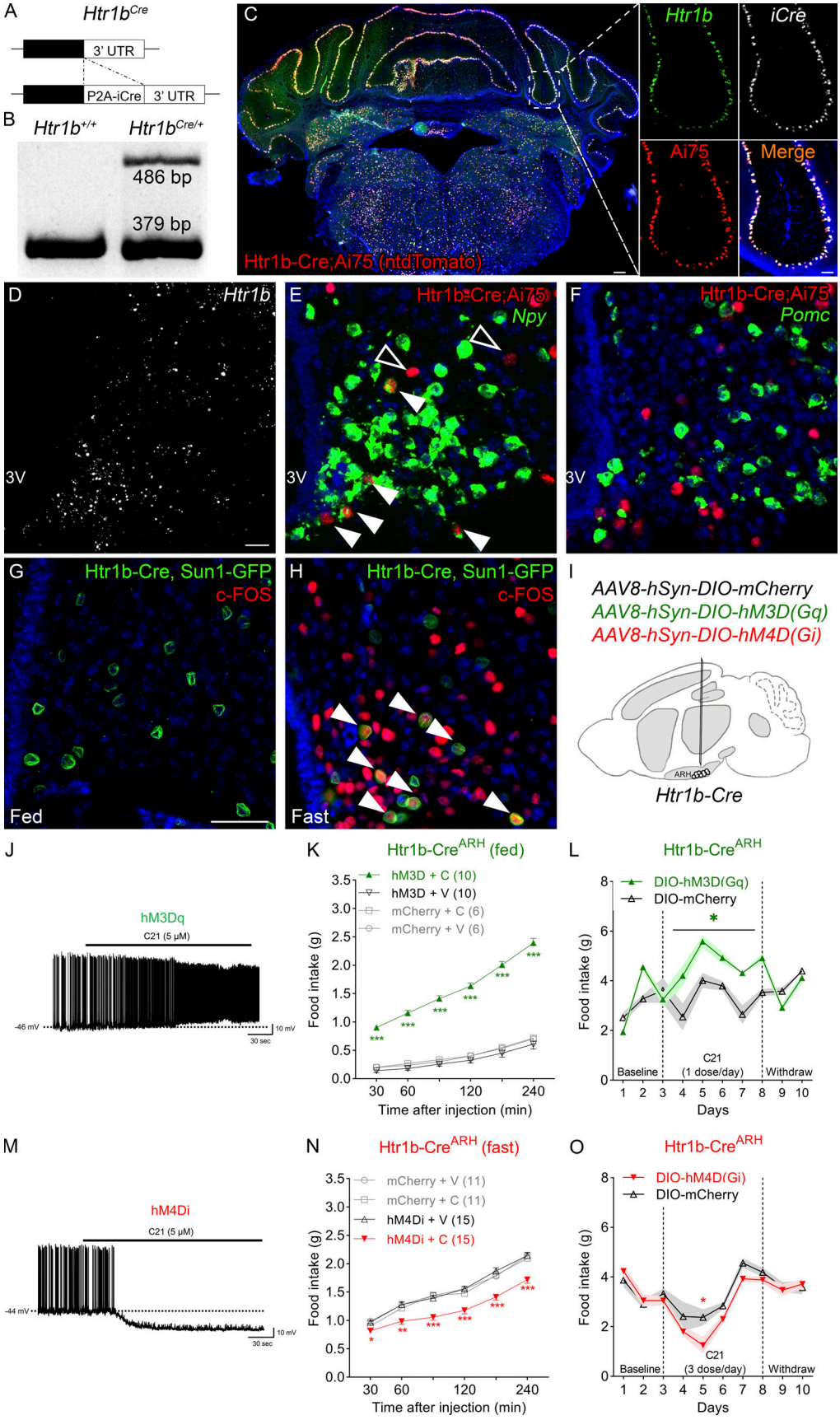

Figure 5. ***Htr1b* marks a subset of *AgRP* neurons that regulates food intake. (A)** Schematic of the *Htr1b*^{WT} (wild-type) and *Htr1b*^{Cre} alleles. **(B)** PCR genotyping of wild-type *Htr1b*$^{+/+}$ and *Htr1b*$^{Cre/+}$ mice. **(C)** Triple-labeling of mRNAs for *Htr1b* (green), *iCre* (white), and proteins for Cre-activated nuclear

tdTomato reporter in cerebellar Purkinje cells. **(D)** RNAscope analysis of *Htr1b* mRNA in the adult ARH. **(E and F)** Dual fluorescence between *Htr1b-Cre* activated nuclear tdTomato (red) and mRNAs (RNAscope, green) for *Npy* (E) and *Pomc* (F). White arrowheads indicate double-labeled neurons Hollow arrowheads indicate *Npy* negative Htr1b neurons. **(G and H)** Dual fluorescence between *Htr1b-Cre* activated nuclear Sun1-GFP (green) and immunostaining for Fos proteins (red) in fed (G) and fasted (H) mice. White arrowheads indicate double-labeled neurons. **(I)** Schematic of stereotaxic bilaterally delivery of AAV viruses containing control, Gq, or Gi DREADD constructs into the ARH of adult *Htr1b-Cre* mice. **(J)** C21 depolarized Htr1b^{ARH} neurons expressing the Gq (hM3Dq) DREADD. **(K and L)** C21 promoted food consumption in mice that expressed Gq (hM3D) DREADD in Htr1b^{ARH} neurons. **(M)** C21 hyperpolarized Htr1b^{ARH} neurons expressing the Gi (hM4Di) DREADD. **(N and O)** C21 inhibited fasting-induced refeeding (N) and daily food intake (O) in mice that expressed Gi (hM4Di) DREADD in Htr1b^{ARH} neurons. Data are presented as mean ± SEM. Two-way ANOVA with Sidak's post hoc tests in K, L, N, and O. *, P < 0.05; **, P < 0.01; and ***, P < 0.001. Scale bars are 20 µm in D–H and 3.8 mm in C. All data were verified in at least two independent experiments.

et al., 2018; Heisler et al., 2002; Xu et al., 2008). In contrast, little is known about the mechanism behind the anorectic actions of Htr1b agonists. This is due, in part, to conflicting literature concerning not only their anorectic effects in mice (Doslikova et al., 2013) but whether or not *Htr1b* is necessary for energy homeostasis (Bouwknecht et al., 2001; Lucas et al., 1998). For example, while several early studies demonstrated a hypophagic effect for CP94253 (Halford and Blundell, 1996; Heisler et al.,

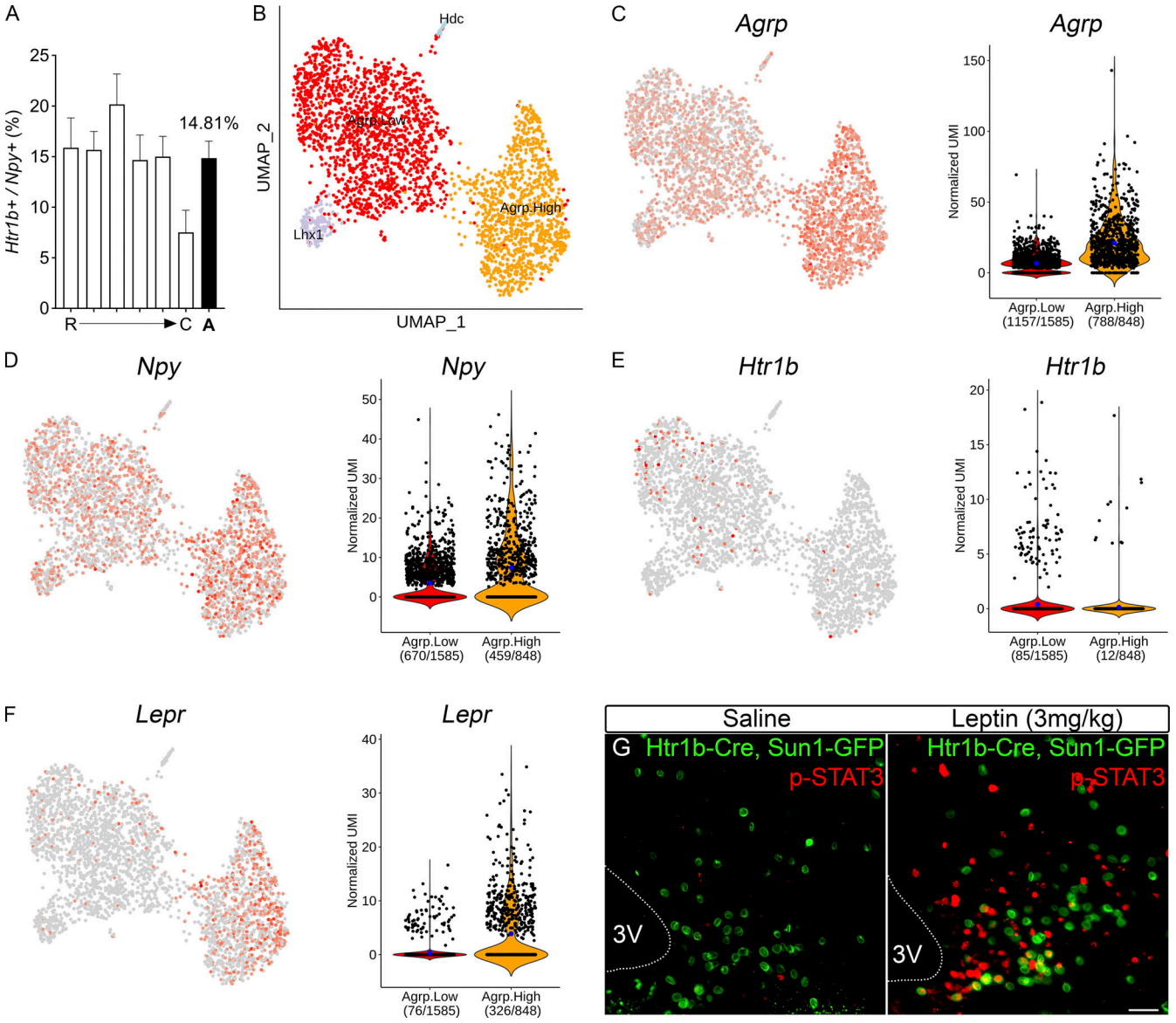

Figure 6. **snRNA-seq analyses of ARH neurons in the adult AgRP-Cre; Sun1-GFP mice. (A)** RNAscope analyses quantifying the percentage of *Npy* mRNA positive ARH neurons expressing *Htr1b* mRNAs. We surveyed adult ARH (every one of 10 serial sections) from three mice across the rostral (R) to caudal (C) axis. The dark column shows the average (A). Data are presented as mean ± SEM. **(B)** Transcriptome-based dimensionality reduction using UMAP identified four putative AgRP clusters. **(C–F)** UMAP and violin plots showing the distribution of *Agrp* (C), *Npy* (D), *Htr1b* (E), and *Lepr* (F) positive cells and their expression levels between the AgRP^{High} and AgRP^{Low} clusters. **(G)** Immunohistochemistry of pSTAT3 (red) in the ARH of *Htr1b-Cre, Sun1-GFP* mice after an IP dose of saline (left) or leptin (3 mg/kg). Scale bars are 20 µm.

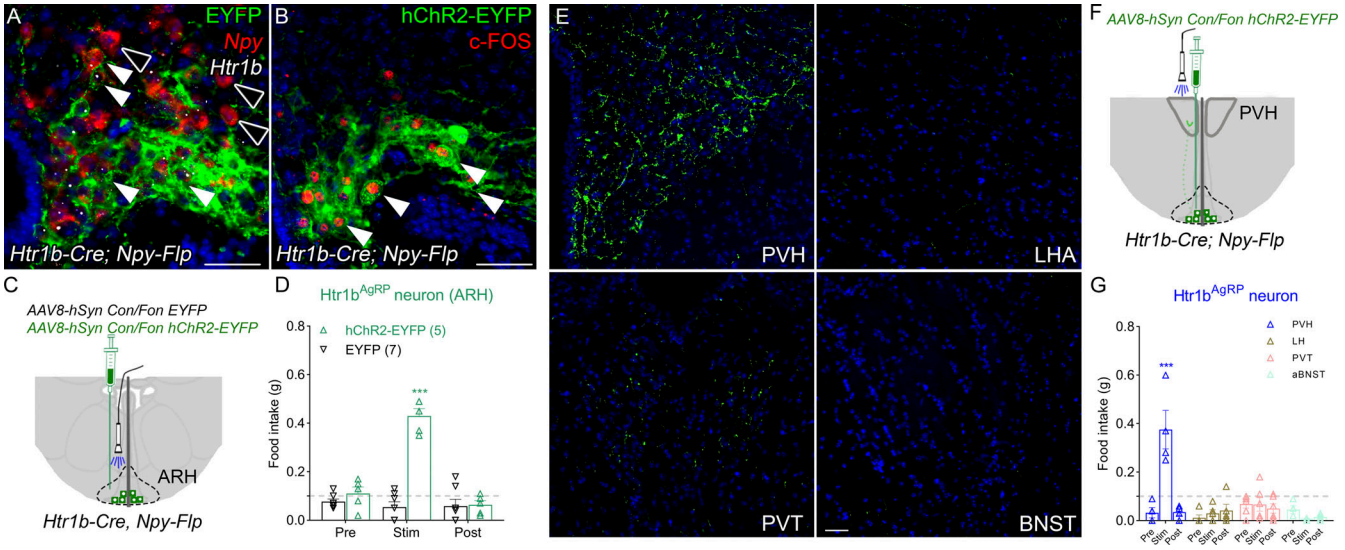

Figure 7. **Htr1b^{AgRP} neurons regulate food intake through a Htr1b$^{AgRP→PVH}$ circuit. (A)** Triple-labeling of EYFP fluorescence (green), *Htr1b* mRNA (white dots, RNAscope), and *Npy* mRNA (red, RNAscope) in the ARH of *Htr1b$^{Cre/+}$*; *Npy$^{Flp/+}$* mice that received AAVs containing Cre- and Flp-dependent EYFP expression cassette. White arrowheads indicate neurons co-express EYFP and *Htr1b*. Hollow arrowheads indicate *Npy* neurons that do not express *Htr1b* or EYFP. **(B)** Dual fluorescence between EYFP (green) and immunostaining for Fos proteins (red) after optical stimulation. White arrowheads indicate double-labeled neurons. **(C)** Schematic of stereotaxic delivery of AAV viruses containing control EYFP or hChR2-EYFP constructs into the ARH of adult *Htr1b-Cre, Npy-Flp* mice. **(D)** Food intake before (pre), during (stim), and after (post) the unilateral optical stimulation of the cell bodies of Htr1b^{AgRP} neurons. **(E)** Immunostaining of EYFP in PVH, LHA, PVT, and BNST. **(F and G)** Food intake before (pre), during (stim), and after (post) the unilateral optical stimulation of Htr1b^{AgRP} neuron axons in the PVH, LH, PVT, and BNST. Data are presented as mean ± SEM. Two-way ANOVA with Sidak's post hoc tests in D and G. ***, P < 0.001. Scale bars are 20 µm. All data were verified in at least two independent experiments.

2006; Lee and Simansky, 1997), a recent analysis found that it failed to suppress food intake in mice even with a high dose (20 mg/kg; Doslikova et al., 2013). Likewise, although one report found normal food intake and body weight in *Htr1b$^{null/null}$* mice (Lucas et al., 1998), another showed hyperphagia and obesity in the same mice (Bouwknecht et al., 2001). We suspected that some inconsistencies could arise from differences in mouse genetic background. As a result, we conducted our analyses in mice on a C57BL/6 background. We found that CP94253 dose-dependently suppressed hunger-induced refeeding in wild-type mice and had a stronger anorectic effect than lorcaserin. Importantly, we showed that its hypophagic effect was independent of *Htr2c* but required endogenous *Htr1b*. Thus, our findings suggest that *Htr1b* and *Htr2c* act on different neural pathways to suppress food intake and can be independently targeted for treating obesity.

Activation of Htr2c suppresses food intake. Consistent with this finding, its loss of function leads to hyperphagic obesity in mice (Berglund et al., 2013; Tecott et al., 1995). In contrast, there seems to be a disconnect between the pharmacological effect of Htr1b activation and its physiological role. Despite the anorectic actions of Htr1b agonists, ablation of Htr1b does not impact food intake or body weight. Of note, Htr1b was deleted during early life in all five knockout mouse models we analyzed. Given its established role during neural development (Bonnin et al., 2007; Dickinson et al., 2016), compensatory adaptations in circuit formation or gene expression may contribute to the lack of a body weight phenotype. To this end, adult ablation studies are warranted to test this hypothesis. Moreover, Htr1b signaling in different brain regions may have an opposing impact on food intake. For example, unlike Htr2c, Htr1b functions as an autoreceptor to regulate 5-HT release. Thus, loss of the $G_{\alpha i}$-coupled Htr1b in adult 5-HT neurons could potentially enhance 5-HT release and indirectly reduce food intake through other 5-HT receptors, which may dampen the effect of its deletion in orexigenic neurons. Collectively, our findings highlight the complex nature of serotonergic regulation of food intake.

Our metabolic phenotyping of C57BL/6 *Htr1b* null mice uncovered a previously unrecognized role for *Htr1b* in postnatal growth. Other than its anorexigenic effect in adult animals, 5-HT plays a pivotal role in early-life growth (Savelieva et al., 2008). Remarkably, the body weight deficits of *Htr1b* null mice resembled those in mice lacking 5-HT during development. For example, mice deficient in tryptophan hydroxylase 2 (*Tph2*), the rate-limiting enzyme for brain 5-HT synthesis, showed similar growth retardation at an early age (Pelosi et al., 2015). Moreover, like *Htr1b* nulls, adult *Tph2* null mice had a modest weight loss compared to their littermate controls (Alenina et al., 2009; Savelieva et al., 2008). It is worth mentioning that little is known regarding how a lack of brain 5-HT signaling leads to a developmental delay in growth. Moreover, specific 5-HT receptors have not been implicated in such deficits. It is possible that 5-HT, acting through *Htr1b*, may have a trophic effect on the maturation of growth-promoting circuits (Bonnin et al., 2007). Alternatively, the absence of 5-HT has been reported to reduce ultrasonic vocalizations in pups (Mosienko et al., 2015), which could indirectly impair parental care. Regardless, our findings reveal a previously unsuspected role for *Htr1b* in mediating 5-HT's effect on these developmental events.

By deleting *Htr1b* in four distinct neuronal populations, we investigated the brain sites that are responsible for its

physiological and pharmacological actions. Our analyses showed that deleting *Htr1b* in 5-HT neurons alone was sufficient to reproduce the growth deficit seen in the null mice. However, the Htr1b autoreceptors were dispensable for the anorectic response to CP94253. In contrast, mice lacking *Htr1b* in the hypothalamus had normal food intake and body weight but no longer responded to CP94253. Collectively, our findings suggest that *Htr1b* engages in spatiotemporally segregated neural pathways to regulate postnatal growth and the anorectic response to 5-HT agents. Of note, our findings did not exclude a potential role for extrahypothalamic *Htr1b*-expressing neurons in food intake. Indeed, it was reported that infusion of d-fenfluramine into the parabrachial nucleus reduces feeding, an event that was blocked by the Htr1b antagonist SB-216641 (Simansky and Nicklous, 2002). Thus, the anorectic effect of Htr1b agonists may involve multiple neural pathways.

Within the hypothalamus, lesions of the PVH did not attenuate d-fenfluramine–induced anorexia (Fletcher et al., 1993). This is consistent with our observation that *Htr1b* in *Sim1* neurons (including those in the PVH) was dispensable for the anorexigenic effect of CP94253. In contrast, such an effect was blunted in mice lacking *Htr1b* in AgRP neurons. Therefore, these results reveal AgRP neurons as one critical site that mediates the hypophagic effect of Htr1b agonists. Within the ARH, our histological analyses detected *Htr1b* mRNAs in both AgRP and non-AgRP neurons. Moreover, we found that some Htr1b^{ARH} neurons were activated by fasting. The development of new *Htr1b-Cre* mice allowed us to chemogenetically manipulate their activities in living mice. This led to our observation that Htr1b^{ARH} neurons can bidirectionally regulate food intake in vivo activation of these neurons to promote food intake, whereas their inhibition suppressed hunger. It is noteworthy that these phenotypes resemble those with similar manipulations of AgRP neurons alone (Krashes et al., 2011). On the other hand, little is known regarding the neurochemical identity of non-AgRP Htr1b^{ARH} neurons, except that they do not express the anorexigenic neuron marker *Pomc*. Moreover, their potential role in feeding regulation remains to be determined.

AgRP neurons regulate many physiological processes and behaviors such as feeding, anxiety, and responses to pain (Alhadeff et al., 2018; Betley et al., 2013; Dietrich et al., 2015). These diverse functions are thought to be carried out by the specific subpopulations of AgRP neurons, each with distinct synaptic inputs and outputs. On the other hand, the cellular and functional heterogeneity of these neurons has just begun to be appreciated. AgRP neurons are innervated by 5-HT neurons and hyperpolarized by 5-HT (Heisler et al., 2006); however, these hyperpolarizing effects are attenuated by pretreatment with a Htr1b antagonist. Our histological analyses revealed that ∼15% of the AgRP neurons express *Htr1b* mRNAs. We suspect that these neurons constitute a subgroup of AgRP neurons that receive 5-HT input and mediate its effects. Interestingly, snRNA-seq analyses demonstrated that the expression of *Htr1b* and the leptin receptors were enriched in two separate subpopulations of AgRP neurons with distinct transcriptomic profiles. Moreover, the sequencing data from ours and others (Campbell et al., 2017) showed that few AgRP neurons co-expressed both transcripts. Notably, it has been reported that 5-HT and leptin act on distinct subpopulations of POMC neurons to regulate energy and glucose metabolism (Sohn et al., 2011). Collectively, these findings raise the possibility that a similar configuration is also adopted by AgRP neurons.

Our intersectional targeting approach enabled us to specifically label the subset of AgRP neurons expressing *Htr1b*. We found that the cell bodies of these neurons were uniquely positioned at the mediobasal part of the ARH. Moreover, unilateral stimulation of the subset of AgRP neurons was sufficient to induce feeding in satiated mice. Interestingly, among the four AgRP neuron targets involved in feeding regulation, the axons of Htr1b^{AgRP} neurons were selectively enriched in the PVH. This suggests that these neurons regulate food intake, in part, through a Htr1b^{AgRP}→PVH circuit. In support of this notion, we found that stimulating the Htr1b^{AgRP} neuron axons at the PVH produced a similar increase in food intake compared to that by cell body stimulations. On the other hand, the source of 5-HT inputs to Htr1b^{AgRP} neurons remained to be determined. Therefore, future studies are warranted to determine the subset of the 5-HT neurons that innervate Htr1b^{ARH} neurons and regulate their function.

Our findings suggest several commonly used, low-cost, antimigraine drugs may also help with weight loss. Indeed, we showed that chronic treatment with frovatriptan reduced food intake and body weight in diet-induced obese mice. Similarly, a loss of appetite has been noted in patients and healthy volunteers taking triptans (Boeles et al., 1997). However, since these drugs are mostly used for treating acute migraine attacks, we suspect that their chronic effects on food intake and body weight might have been under-recognized. We have demonstrated that the anorectic effect of frovatriptan depended on *Htr1b*. Notably, like other 5-HT–based medications, a common concern for the chronic use of triptans is that it may lead to increased risks for adverse cardiovascular events. In particular, the first generation of triptans, such as sumatriptan, can cause vasoconstriction and acutely increase blood pressure (Vanmolkot and de Hoon, 2006). In contrast, new generation triptans like frovatriptan had no effect on blood pressure or heart rate (Parsons et al., 1998; Saracheva et al., 2020). Furthermore, multiple clinical studies evaluating the cardiac safety of these drugs have shown they were relatively safe after frequent and long-term use even in patients with arterial hypertension or coronary artery disease (Elkind et al., 2004; Robbins, 2004; Tullo et al., 2013). Finally, triptans demonstrate only partial agonistic properties for Htr1b. Thus, it is possible that compounds with higher specificity (e.g., CP94253) may produce a stronger anorectic effect. Moreover, CP94253 reduces food intake in rats without perturbing their characteristic behavioral sequences that reflect the onset of satiety (Lee and Simansky, 1997). Therefore, future work is warranted to comprehensively evaluate the effects of additional Htr1b-specific agonists on appetite, body weight, and safety. In summary, by illustrating a neural pathway for appetite suppression, our findings suggest that *Htr1b* is a new target for 5-HT–based weight-loss therapies.

Materials and methods

All mice were housed in a temperature-controlled room with a 12-h light/12-h dark cycle (lights on at 6 a.m., lights off at 6 p.m.)

in the animal facility of UT Southwestern (UTSW) Medical Center. Mice were provided standard chow (No. 2016; Harlan Teklad) as well as water ad libitum unless otherwise noted. For the HFD experiment, mice were fed #D12492 (20% kcal protein, 20% kcal carbohydrate, and 60% kcal fat, Research Diets).

All mice were maintained on a C57BL/6 background. Wild-type C57Bl/6J (000664; JAX), *Pet1-Cre* (012712; JAX), *Foxd1-Cre* (012463; JAX), *Agrp-Cre* (012899; JAX), *Npy-flp* (030211; JAX), Ai75 (ROSA26Sor$^{[RCL\text{-}nls\ tdT]\text{-}D}$; 025106; JAX), Ai14 (ROSA26Sor$^{[RCL\text{-}tdT]\text{-}D}$; 007914; JAX), and Sun1-sfGFP (ROSA26Sor$^{CAG\text{-}Sun1/sfGFP}$; 021039; JAX) mice were obtained from The Jackson Laboratory (JAX). *Htr1b-flox* (5752473; Mouse Genome Informatics [MGI]) and *Htr1b-null* (2653030; MGI) mice were obtained from René Hen's lab at Columbia University. *Sim1-Cre* (3692526; MGI) and *Mc4r*$^{flox/flox}$ (5484615; MGI) mice were obtained from Bradford Lowell's lab at Beth Israel Deaconess Medical Center and Harvard Medical School, Boston, MA. *Htr2c-null* (3841486; MGI) mice were obtained from Joel Elmquist's lab at UTSW Medical Center, Dallas, TX. *Htr1b-Cre* mice were made and characterized in the current study.

All the mouse experiments were approved by the Institutional Animal Care and Use Committee of the UTSW Medical Center.

Metabolic phenotype analysis

A magnetic-resonance whole-body composition analyzer (EchoMRI) was used to determine body composition (fat mass, lean mass, and water content). Energy intake, expenditure, and physical activity were assessed using an indirect calorimetric system (TSE PhenoMaster) at the UTSW Medical Center Metabolic Phenotyping Core.

Immunohistochemistry and RNAscope

Mouse brains were fixed in 4% paraformaldehyde overnight and then placed in a 30% sucrose solution for cryoprotection. The primary antibodies used include anti-GFP (rabbit, #ab290; Abcam), anti-GFP (chicken, #GFP-1020; Aves Labs), anti-RFP (rabbit, #600-401-379; Rockland), anti-c-fos (rabbit, #ab190289; Abcam), and anti-pSTAT3 (rabbit, #9145; Cell Signaling Technology). For pSTAT3 immunohistochemistry, sections were pre-incubated with 1% NaOH for 20 min, followed by 10 min with 0.3% glycine–PBS and 10 min with 0.03% SDS–PBS solution before transfer to primary antibody buffer. All Alexa Fluor–conjugated secondary antibodies were from Invitrogen.

RNAscope experiments were performed using the Multiplex Fluorescent Detection Kit version 2 (Cat# 323100) from Advanced Cell Diagnostics following the manufacturer's protocol. The RNA probes used include Mm-Pomc (Cat# 314081), Mm-Npy (Cat# 313321), Mm-Htr1b (Cat# 315861), and iCre (Cat# 423321). All fluorescence images were acquired using the Zeiss LSM880 Airyscan confocal microscope.

GTT

For the GTT, mice were fasted for 8 h with water provided ad libitum from 8 a.m. on the experimental day. During GTT, blood glucose levels were monitored at 0, 15, 30, 60, 90, and 120 min after an IP dose of glucose (dextrose; 1.0 g/kg body weight). Blood glucose was taken from the tail vein and analyzed using a glucometer (Li et al., 2021b; Johnson & Johnson).

qPCR

Total RNA was isolated using the Direct-zol RNA Kit (Zymo) according to the manufacturer's recommendations. 3 µg of total RNA were used as the template for cDNA synthesis (Invitrogen). Real-time PCR was performed using the TaqMan Universal PCR Master Mix (Thermo Fisher Scientific). qPCR reactions were carried out in triplicate using the 384-well PCR microplate for CFX384 Touch Real-Time PCR Detection System (Bio-Rad). Taqman probes used include (*Agrp*, Mm00475829_g1; *Htr1b*, Mm00439377_s1; *Htr2c*, Mm00434127_m1; *Npy*, Mm01410146_m1; *Htr1a*, Mm00434106_m1; *Tph2*, Mm00557715_m1; *Pet1*, Mm00462220_m1; and *Tbp*, Mm00446973_m1; Thermo Fisher Scientific). The relative expression levels of each gene were normalized to the housekeeping gene TATA-box binding protein (*Tbp*), and the specificity of amplified DNA products was verified by examining dissociation curves. RNA expression data were analyzed using the $-\Delta\Delta C_t$ method.

Stereotaxic surgery

Male mice (at least 8 wk old) were anesthetized with 1.5% isoflurane and placed on a stereotaxic frame (David Kopf Instruments). After the skull was exposed and leveled in the horizontal plane, small holes were drilled into the skull for viral infections or fiber implantation. AAV was bilaterally injected into the arcuate nucleus (anteroposterior [AP], –1.30 mm; mediolateral [ML], ±0.25 mm; dorsoventral [DV], –5.95 mm). A total of 210 nl of the virus was injected at a rate of 30 nl/min and was allowed 8–10 min to diffuse before the injection needle was removed. AAV vectors used include AAV8-hSyn-DIO-mCherry (#50459; Addgene), AAV8-hSyn-DIO-hM3D(Gq)-mCherry (#44361; Addgene), AAV8-hSyn-DIO-hM4D(Gi)-mCherry (#44362; Addgene), AAV8-hSyn Con/Fon EYFP (#55650; Addgene), and AAV8-hSyn Con/Fon hChR2(H134R)-EYFP (#55645; Addgene).

A ferrule-capped fiber (ferrule inner diameter 230 µm, Cat# FZI-LC-230; Kientec Systems) was unilaterally implanted for photostimulation. Region coordinates used: ARH at AP, –1.30 mm; ML, –0.10 mm; DV, –5.80 mm; PVH at AP, –0.50 mm; ML, –0.10 mm; DV, –4.60 mm; PVT at AP, –1.25 mm; ML, 0 mm; DV, –2.60 mm; LHA at AP, –1.20 mm; ML, –1.40 mm; DV, –4.60 mm; aBNST at AP, +0.40 mm; ML, –0.50 mm; DV, –4.10 mm. Dental cement (Parkell) was used to fix the ferrule-capped fibers to the skull. After surgery, mice were allowed to recover for at least 4 wk before the behavioral tests. As we have done in the past (Yoo et al., 2021), the injection site was verified for each mouse using Cre- and/or Flp-dependent fluorescent reporters. As a result, two mice (2/58) were excluded from the chromogenic experiments and six mice (6/38) were excluded from the optogenetic experiments.

Feeding studies

Mice were fasted for 18 h (from 4 p.m. to 10 a.m.) before being given an IP dose of CP94253 hydrochloride (Cat# 1945; Axon Medchem LLC), lorcaserin hydrochloride (Cat# A12598-50; Adooq Bioscience), eletriptan hydrobromide (A11418-10; Adooq

Bioscience), almotriptan malate (Cat# A11799-10; Adooq Bioscience), naratriptan hydrochloride (Cat# HY-B0197A; MedChemExpress), rizatriptan benzoate (Cat# SML0247; Sigma-Aldrich), frovatriptan succinate (Cat# SML1291; Sigma-Aldrich), zolmitriptan (Cat# SML0248; Sigma-Aldrich). 30 min after the injection, a chow pellet was given to singly housed mice. Food consumption was monitored at 30, 60, 120, and 240 min afterward. Individual mouse's responses to different drugs were determined by crossover refeeding experiments conducted 1 wk apart from each other.

In the chemogenetic studies, all mice were singly housed for 3 to 4 wk after the AAV injection. The day before the experiment, mice were placed in new cages to avoid food crumbs trapped in the bedding. Fed or fasted mice were given an IP dose of C21 (DREADD agonist 21, SML2392; Sigma-Aldrich, 1 mg/kg of body weight) or 0.9% saline (vehicle) at 10 a.m. Food consumption was measured at 30, 60, 120, and 240 min afterward. Daily food intake was measured at 4 p.m. C21 was injected once per day in the hM3Dq group and three times (4 p.m., 12 p.m., and 8 a.m.) in the hM4Di group.

In the photostimulation experiments, all mice were singly housed for 3 to 4 wk following the surgery. The day before the experiment, mice were placed in new cages to avoid food crumbs trapped in the bedding. Mice then were attached to fiber optic cables (Cat# OPT/PC-LC-LCF-200/230; Plexon) and the other end of the optic fiber was connected to an LED. During the 1-h stimulation period, the mice were exposed to ∼6 mW blue light stimulation (473 nm). We used the same stimulation protocol as described previously (Betley et al., 2013): 10 ms pulses, 20 Hz for 1 s, repeated every 4 s for 1 h. Food consumption was measured 60 min before, during, and after photostimulation.

snRNA-seq and bioinformatics

The snRNA-seq protocol was adapted from others' (Gaublomme et al., 2019; Stoeckius et al., 2018). 15 mouse hypothalami were dissected and stored at −80°C. Each sample was separately homogenized with 1 ml lysis buffer (0.10% NP40 [492018; Sigma-Aldrich]; 0.02% Tween20 [P9416; Sigma-Aldrich], 1% BSA [A7979; Sigma-Aldrich], 1 mM dithiothreitol [646563; Sigma-Aldrich], 1 U/µl RNase inhibitor [3335402001; Sigma-Aldrich], 10 mM Tris-Hydrochloride [T2194; Sigma-Aldrich], magnesium chloride [M1028; Sigma-Aldrich] and sodium chloride [5922C; Sigma-Aldrich]) in a 2-ml dounce homogenizer. After 20 times dounce, the lysis solution was filtered through a 30-µm filter (130-041-407; Milentyi Biotec). The homogenizer was rinsed twice with 1 ml wash buffer (0.02% Tween20, 1% BSA, 1 mM dithiothreitol, 0.1 U/µl RNase inhibitor, 10 mM Tris-hydrochloride, magnesium chloride, and sodium chloride). The wash solution was filtered and added to the homogenate. The homogenate solution was then centrifuged at 500 *g* for 5 min in a swing bucket rotor and the supernatant was removed. The homogenate pellet was resuspended in 100 µl of wash buffer. After that, 10 µl Fc Blocking reagent (Cat# 156604; BioLegend) was added for 5 min. The resuspended nuclei samples were then incubated with different TotalSeq Hashtag antibodies against the nuclear pore complex (0.5 µl, MAb414; BioLegend) for 10 min. The nuclei suspensions were washed three times with 1 ml wash buffer and spun down again at 500 *g* for 5 min. After hashtagging each sample with the antibody, all samples were pooled together, and GFP positive nuclei were sorted on a FACSAria machine at the Flow Cytometry Core of UTSW Medical Center. After sorting, the nuclei solution was adjusted to the desired concentration at 500–2,000 nuclei/µl then proceeded with the 10× Genomics single-cell 3′ v3 assay. Nuclei and reagents were prepared and loaded onto the chip and into the Chromium Controller for droplet generation. Reverse transcription was conducted in the droplets and cDNA was recovered through demulsification and bead purification. Pre-amplified cDNA was used for library preparation and multiplexed. All procedures mentioned above were performed on ice or in a cold room at all times.

Each hashtag oligonucleotide (HTO) containing library was prepared as described by others and the Cite-seq website (Gaublomme et al., 2019; Stoeckius et al., 2018). Briefly, 2 pmol of HTO additive oligonucleotides (5′-GTGACTGGAGTTCAGACG TGTGCTC-3′) were added during the cDNA amplification step. cDNA was amplified according to the 10× Single Cell 3′ v3 protocol. After PCR amplification, cell HTO-containing fraction in the supernatant was separated via 0.6× SPRI (solid phase reversible immobilization). The cDNA fraction continued to be processed according to the 10× Genomics Single Cell 3′ v3 protocol to generate the transcriptome library. An additional 1.4× reaction volume of SPRI beads was added to the HTO fraction (2.0×). The beads were washed and eluted. We performed the second round of 2.0× SPRI selection. After the final elution, the HTO library was generated by the following PCR program (95°C, 3 min; 12 cycles of [95°C, 20 s, 64°C 30 s, 72° 20 s], 72°C, 5 min) with the HTO primer sets (SI-PCR, 5′-AATGATACGGCGACCACC GAGATCTACACTCTTTCCCTACACGACGC*T*C-3′; D709_s, 5′-CAAGCAGAAGACGGCATACGAGATAGCTTCAGGTGACTGGAG TTCAGACGTGT*G*C-3′). The 10 × 3′ library and HTO library were sequenced on a NextSeq 2000 mid-throughput sequencing platform.

HTO samples were demultiplexed using Seurat-based HTODemux. Hashtag-count matrix was generated from sequenced hashtag fastq reads using CITE-seq-count v1.4 (https://hoohm.github.io/CITE-seq-Count/) with the following parameters: -t antibody_index.csv -wl 737K-august-2016.txt -cbf 1 -cbl 16 -umif 17 -umil 26. In the parameter list, antibody_index.csv maps sample-specific hashtag barcodes to sample names. Next, we ran Seurat's HTODemux on the hashtag-count matrix to demultiplex cell barcode of interest.

Sequencing data in the binary base call format were demultiplexed. UMI counts were obtained by aligning FASTQ files to the mouse reference genome (mm10) using Cell Ranger software (version 6.0.0) from 10× Genomics. Sequential analysis was conducted using Seurat v4 package (Hao et al., 2021). Cells meeting the following quality control parameters were included in the analyses: (1) number of detected genes >500 and ≤6,000); (2) the percentage of mitochondrial gene expression <5% per cell; (3) genes expressed in at least 10 cells were included; (4) cells with singlets signature from HTODemux. We scaled UMI counts by normalizing library size to 10,000. The normalized expression values were then log-transformed. Following the application of these filters, 3,456 nuclei passed quality control. We scaled UMI counts by normalizing each library size to 10,000.

The normalized expression values were then log-transformed. The 2,000 most highly variable genes as measured by dispersion were selected for the computation of principal components (PCs). Before the computation of PCs, mitochondrial genes and the gender-specific gene *Xist* were excluded from this set of highly variable genes. PC analysis was then performed on normalized expression values on the first 50 PCs. An elbow plot was inspected to determine the appropriate number of top PCs capturing the most variances. Using this approach, we selected the first 20 PCs for further analyses. UMAP analysis was performed using the "uwot" function on the embedded matrix derived from the first 20 PCs and 30 neighbors using cosine as the metric parameter. Cells were clustered using the k-nearest neighbor approach, using the Euclidean metric as the input parameter. The weighted graph was created with the weight values calculated from the normalized shared number of the nearest neighbors. Identified clusters were superimposed on the two-dimensional UMAP. We identified five clusters expressing gene signatures corresponding to non-neural cells (vascular cells, $n = 77$ cells; astrocytes, $n = 255$ cells; microglia, $n = 34$ cells; two oligodendrocytes' populations, $n = 83$ and 155 cells) and we removed these clusters from further analyses.

Electrophysiology

Whole-cell patch-clamp recordings on Htr1b^{ARH} neurons were conducted on the hypothalamic slice prepared from *Htr1b-P2A-iCre* mice that received injections of AAV8-hSyn-DIO-hM3D(Gq)-mCherry or AAV8-hSyn-DIO-hM4D(Gi)-mCherry. The data analyses were performed as previously described (Sohn et al., 2016). Briefly, AAV-injected mice were deeply anesthetized with isoflurane inhalations and transcardially perfused with a modified ice-cold artificial CSF (ACSF; described below), in which an equimolar amount of sucrose was substituted for NaCl. The mice were then decapitated, and the entire brain was removed and immediately submerged in ice-cold, carbogen-saturated (95% O_2 and 5% CO_2) ACSF (126 mM NaCl, 2.8 mM KCl, 1.2 mM $MgSO_4$, 2.5 mM $CaCl_2$, 1.25 mM NaH_2PO_4, 26 mM $NaHCO_3$, and 5 mM glucose). A brain block containing the hypothalamus was made. Coronal sections (250 µm) were cut with a Leica VT1200S Vibratome and then incubated in oxygenated ACSF at room temperature for at least 1 h for recovery. Slices were transferred to the recording chamber and allowed to equilibrate for 10–20 min before recording. The slices were bathed in oxygenated ACSF (32–34°C) at a flow rate of ∼2 ml/min. The pipette solution was modified for whole-cell recording: 120 mM K-gluconate, 10 mM KCl, 10 mM Hepes, 5 mM EGTA, 1 mM $CaCl_2$, 1 mM $MgCl_2$, and 2 mM MgATP, pH 7.3. Electrophysiological signals were recorded using an Axopatch 700B amplifier (Molecular Devices), low-pass filtered at 2–5 kHz, and analyzed offline on a PC with pCLAMP programs (Molecular Devices). Recording electrodes had resistances of 4–6 MΩ when filled with the K-gluconate internal solution. Input resistance was assessed by measuring voltage deflection at the end of the response to a hyperpolarizing rectangular current pulse steps (500 ms of −25 to 0 pA). Membrane potential values were not compensated to account for junction potential (−8 mV). Solutions containing 5 µM C21 were typically perfused for ∼5 min. A drug effect was required to be associated temporally with peptide application, and the response had to be stable within a few minutes. A neuron was considered depolarized or hyperpolarized if a change in membrane potential was at least 2 mV in amplitude.

Quantification and statistical analyses

Replicate information is indicated in the figure legends. All results are given as mean ± SEM and analyzed by using statistical tools implemented in Prism (GraphPad version 9). Statistical analyses were performed using the Student's *t* test and regular one-way or two-way ANOVA. Repeated-measures ANOVA was used to compare changes in variables (e.g., food intake, body weight, blood glucose) over time, one-way ANOVA was used to assess the effects of one variable (e.g., genotype) on a parameter, or two-way ANOVA to assess effects of two variables on a parameter, as needed, followed by Sidak's post-hoc analysis for P values <0.05. The F values from the two-way ANOVA analyses reflect interactions between genotype × treatment/dose, whereas the asterisks represent P values between groups. Differences with $P < 0.05$ were considered to be significant. $P < 0.05$ (*), $P < 0.01$ (**), and $P < 0.001$ (***).

Online supplementary material

Fig. S1 shows the anorexigenic effect of CP94235 and lorcaserin in a fast-refeeding test. Fig. S2 shows the validation of deletion of *Htr1b* in *Htr1b*$^{Pet1\text{-}KO}$ and *Htr1b*$^{Foxd1\text{-}KO}$ mice. Fig. S3 shows normal body weight in *Htr1b*$^{Sim1\text{-}KO}$ and *Htr1b*$^{Agrp\text{-}KO}$ mice. Fig. S4 shows additional snRNA-seq analyses of ARH neurons in the adult AgRP-Cre; Sun1-GFP mice. Fig. S5 shows the validation of Cre- and Flp-dependent hChR2-EYFP expression.

Data availability

The transcriptomics data is now deposited at GEO (the accession number for the transcriptomics data is GSE199062).

Acknowledgments

We thank the members of the UTSW Metabolic Phenotyping Core. We thank UTSW Live Cell Imaging Facility for providing Zeiss LSM880 Airyscan confocal microscope; the instrument is funded by National Institutes of Health 1S10OD021684-01 to Kate Luby-Phelps. We thank Dr. Syann Lee and other members of the UTSW Metabolic Phenotyping Core. We thank Caitlin Eaton and Yaroslav Bisikalo at UTSW Next Generation Sequencing Core. We also thank Dr. Kimberly Cox at Efferent Manuscript Services for her assistance in preparing the manuscript for publication.

The authors were supported by U.S. National Institutes of Health grants R01 DK114036, DK130892 to C. Liu; F32DK116427 to S.C. Wyler; and K01AA024809 to L. Jia; and Korean National Research Foundation grants 2019R1A2C2005161, 2022R1A2C3005613 to J.-W. Sohn. C. Liu was also supported by American Heart Association Scientist Development Grant 16SDG27260001, a UTSW Pilot & Feasibility Award, and a Grossman Endowment Award for Excellence in Diabetes Research.

Author contributions: L. Li and C. Liu designed the experiments. L. Li, S.C. Wyler, L.A. León-Mercado, Y. Oh, Swati, X.M.

Chen, R. Wan, A.G. Arnold, G. Wang, L. Jia, and J.-W. Sohn collected data. L. Li, J.-W. Sohn, and C. Liu analyzed the data. K. Nautiyal and R. Hen provided essential reagents and suggestions that improved the manuscript. L. Li, J.-W. Sohn, and C. Liu wrote the manuscript.

Disclosures: The authors declare no competing interests exist.

Submitted: 3 January 2022
Revised: 4 April 2022
Accepted: 13 June 2022

References

Alenina, N., D. Kikic, M. Todiras, V. Mosienko, F. Qadri, R. Plehm, P. Boye, L. Vilianovitch, R. Sohr, K. Tenner, et al. 2009. Growth retardation and altered autonomic control in mice lacking brain serotonin. *Proc. Natl. Acad. Sci. USA*. 106:10332–10337. https://doi.org/10.1073/pnas.0810793106

Alhadeff, A.L., Z. Su, E. Hernandez, M.L. Klima, S.Z. Phillips, R.A. Holland, C. Guo, A.W. Hantman, B.C. De Jonghe, and J.N. Betley. 2018. A neural circuit for the suppression of pain by a competing need state. *Cell*. 173:140–152.e15. https://doi.org/10.1016/j.cell.2018.02.057

Balthasar, N., L.T. Dalgaard, C.E. Lee, J. Yu, H. Funahashi, T. Williams, M. Ferreira, V. Tang, R.A. McGovern, C.D. Kenny, et al. 2005. Divergence of melanocortin pathways in the control of food intake and energy expenditure. *Cell*. 123:493–505. https://doi.org/10.1016/j.cell.2005.08.035

Becht, E., L. McInnes, J. Healy, C.A. Dutertre, I.W.H. Kwok, L.G. Ng, F. Ginhoux, and E.W. Newell. 2018. Dimensionality reduction for visualizing single-cell data using UMAP. *Nat. Biotechnol.* https://doi.org/10.1038/nbt.4314

Berglund, E.D., C. Liu, J.W. Sohn, T. Liu, M.H. Kim, C.E. Lee, C.R. Vianna, K.W. Williams, Y. Xu, and J.K. Elmquist. 2013. Serotonin 2C receptors in pro-opiomelanocortin neurons regulate energy and glucose homeostasis. *J. Clin. Invest.* 123:5061–5070. https://doi.org/10.1172/JCI70338

Betley, J.N., Z.F. Cao, K.D. Ritola, and S.M. Sternson. 2013. Parallel, redundant circuit organization for homeostatic control of feeding behavior. *Cell*. 155:1337–1350. https://doi.org/10.1016/j.cell.2013.11.002

Boeles, S., C. Williams, G.M. Campling, E.M. Goodall, and P.J. Cowen. 1997. Sumatriptan decreases food intake and increases plasma growth hormone in healthy women. *Psychopharmacology*. 129:179–182. https://doi.org/10.1007/s002130050178

Bonnin, A., M. Torii, L. Wang, P. Rakic, and P. Levitt. 2007. Serotonin modulates the response of embryonic thalamocortical axons to netrin-1. *Nat. Neurosci.* 10:588–597. https://doi.org/10.1038/nn1896

Bouwknecht, J.A., J. van der Gugten, T.H. Hijzen, R.A. Maes, R. Hen, and B. Olivier. 2001. Male and female 5-HT(1B) receptor knockout mice have higher body weights than wildtypes. *Physiol. Behav.* 74:507–516. https://doi.org/10.1016/s0031-9384(01)00589-3

Bovetto, S., and D. Richard. 1995. Functional assessment of the 5-HT 1A-1B-2A/2C-and 3-receptor subtypes on food intake and metabolic rate in rats. *Am. J. Physiol.* 268:R14–R20. https://doi.org/10.1152/ajpregu.1995.268.1.R14

Campbell, J.N., E.Z. Macosko, H. Fenselau, T.H. Pers, A. Lyubetskaya, D. Tenen, M. Goldman, A.M. Verstegen, J.M. Resch, S.A. McCarroll, et al. 2017. A molecular census of arcuate hypothalamus and median eminence cell types. *Nat. Neurosci.* 20:484–496. https://doi.org/10.1038/nn.4495

Colman, E., J. Golden, M. Roberts, A. Egan, J. Weaver, and C. Rosebraugh. 2012. The FDA's assessment of two drugs for chronic weight management. *N. Engl. J. Med.* 367:1577–1579. https://doi.org/10.1056/NEJMp1211277

Connolly, H.M., J.L. Crary, M.D. McGoon, D.D. Hensrud, B.S. Edwards, W.D. Edwards, and H.V. Schaff. 1997. Valvular heart disease associated with fenfluramine-phentermine. *N. Engl. J. Med.* 337:581–588. https://doi.org/10.1056/NEJM199708283370901

D'Agostino, G., D. Lyons, C. Cristiano, M. Lettieri, C. Olarte-Sanchez, L.K. Burke, M. Greenwald-Yarnell, C. Cansell, B. Doslikova, T. Georgescu, et al. 2018. Nucleus of the solitary tract serotonin 5-HT2C receptors modulate food intake. *Cell Metabol.* 28:619–630.e5. https://doi.org/10.1016/j.cmet.2018.07.017

Dickinson, M.E., A.M. Flenniken, X. Ji, L. Teboul, M.D. Wong, J.K. White, T.F. Meehan, W.J. Weninger, H. Westerberg, H. Adissu, et al. 2016. High-throughput discovery of novel developmental phenotypes. *Nature*. 537:508–514. https://doi.org/10.1038/nature19356

Dietrich, M.O., M.R. Zimmer, J. Bober, and T.L. Horvath. 2015. Hypothalamic Agrp neurons drive stereotypic behaviors beyond feeding. *Cell*. 160:1222–1232. https://doi.org/10.1016/j.cell.2015.02.024

Doslikova, B., A.S. Garfield, J. Shaw, M.L. Evans, D. Burdakov, B. Billups, and L.K. Heisler. 2013. 5-HT2C receptor agonist anorectic efficacy potentiated by 5-HT1B receptor agonist coapplication: An effect mediated via increased proportion of pro-opiomelanocortin neurons activated. *J. Neurosci.* 33:9800–9804. https://doi.org/10.1523/JNEUROSCI.4326-12.2013

Elkind, A.H., L.Z. Satin, A. Nila, and C. Keywood. 2004. Frovatriptan use in migraineurs with or at high risk of coronary artery disease. *Headache*. 44:403–410. https://doi.org/10.1111/j.1526-4610.2004.04071.x

Fenno, L.E., J. Mattis, C. Ramakrishnan, M. Hyun, S.Y. Lee, M. He, J. Tucciarone, A. Selimbeyoglu, A. Berndt, L. Grosenick, et al. 2014. Targeting cells with single vectors using multiple-feature Boolean logic. *Nat. Methods*. 11:763–772. https://doi.org/10.1038/nmeth.2996

Fletcher, P.J., P.J. Currie, J.W. Chambers, and D.V. Coscina. 1993. Radiofrequency lesions of the PVN fail to modify the effects of serotonergic drugs on food intake. *Brain Res.* 630:1–9. https://doi.org/10.1016/0006-8993(93)90635-z

Gaublomme, J.T., B. Li, C. McCabe, A. Knecht, Y. Yang, E. Drokhlyansky, N. Van Wittenberghe, J. Waldman, D. Dionne, L. Nguyen, et al. 2019. Nuclei multiplexing with barcoded antibodies for single-nucleus genomics. *Nat. Commun.* 10:2907. https://doi.org/10.1038/s41467-019-10756-2

Ghanshani, S., C. Chen, B. Lin, L. Duan, Y.A. Shen, and M.S. Lee. 2020. Risk of acute myocardial infarction, heart failure, and death in migraine patients treated with triptans. *Headache*. 60:2166–2175. https://doi.org/10.1111/head.13959

Halford, J.C., and J.E. Blundell. 1996. The 5-HT1B receptor agonist CP-94, 253 reduces food intake and preserves the behavioural satiety sequence. *Physiol. Behav.* 60:933–939. https://doi.org/10.1016/0031-9384(96)00073-x

Hao, Y., S. Hao, E. Andersen-Nissen, W.M. Mauck 3rd, S. Zheng, A. Butler, M.J. Lee, A.J. Wilk, C. Darby, M. Zager, et al. 2021. Integrated analysis of multimodal single-cell data. *Cell*. 184:3573–3587.e29. https://doi.org/10.1016/j.cell.2021.04.048

Heisler, L.K., M.A. Cowley, L.H. Tecott, W. Fan, M.J. Low, J.L. Smart, M. Rubinstein, J.B. Tatro, J.N. Marcus, H. Holstege, et al. 2002. Activation of central melanocortin pathways by fenfluramine. *Science*. 297:609–611. https://doi.org/10.1126/science.1072327

Heisler, L.K., E.E. Jobst, G.M. Sutton, L. Zhou, E. Borok, Z. Thornton-Jones, H.Y. Liu, J.M. Zigman, N. Balthasar, T. Kishi, et al. 2006. Serotonin reciprocally regulates melanocortin neurons to modulate food intake. *Neuron*. 51:239–249. https://doi.org/10.1016/j.neuron.2006.06.004

Hikiji, K., K. Inoue, S. Iwasaki, K. Ichihara, and N. Kiriike. 2004. Local perfusion of mCPP into ventromedial hypothalamic nucleus, but not into lateral hypothalamic area and frontal cortex, inhibits food intake in rats. *Psychopharmacology*. 174:190–196. https://doi.org/10.1007/s00213-003-1735-0

Hutson, P.H., T.P. Donohoe, and G. Curzon. 1988. Infusion of the 5-hydroxytryptamine agonists RU24969 and TFMPP into the paraventricular nucleus of the hypothalamus causes hypophagia. *Psychopharmacology*. 95:550–552. https://doi.org/10.1007/BF00172974

Krashes, M.J., S. Koda, C. Ye, S.C. Rogan, A.C. Adams, D.S. Cusher, E. Maratos-Flier, B.L. Roth, and B.B. Lowell. 2011. Rapid, reversible activation of AgRP neurons drives feeding behavior in mice. *J. Clin. Invest.* 121:1424–1428. https://doi.org/10.1172/JCI46229

Lee, M.D., and K.J. Simansky. 1997. CP-94, 253: A selective serotonin1B (5-HT1B) agonist that promotes satiety. *Psychopharmacology*. 131:264–270. https://doi.org/10.1007/s002130050292

Lein, E.S., M.J. Hawrylycz, N. Ao, M. Ayres, A. Bensinger, A. Bernard, A.F. Boe, M.S. Boguski, K.S. Brockway, E.J. Byrnes, et al. 2007. Genome-wide atlas of gene expression in the adult mouse brain. *Nature*. 445:168–176. https://doi.org/10.1038/nature05453

Li, L., E.S. Yoo, X. Li, S.C. Wyler, X. Chen, R. Wan, A.G. Arnold, S.G. Birnbaum, L. Jia, J.W. Sohn, and C. Liu. 2021a. The atypical antipsychotic risperidone targets hypothalamic melanocortin 4 receptors to cause weight gain. *J. Exp. Med.* 218:e20202484. https://doi.org/10.1084/jem.20202484

Li, M., L. Li, B. Li, C. Hambly, G. Wang, Y. Wu, Z. Jin, A. Wang, C. Niu, C. Wolfrum, and J.R. Speakman. 2021b. Brown adipose tissue is the key depot for glucose clearance in microbiota depleted mice. *Nat. Commun.* 12:4725. https://doi.org/10.1038/s41467-021-24659-8

Liu, C., T. Maejima, S.C. Wyler, G. Casadesus, S. Herlitze, and E.S. Deneris. 2010. Pet-1 is required across different stages of life to regulate serotonergic function. *Nat. Neurosci.* 13:1190–1198. https://doi.org/10.1038/nn.2623

Lucas, J.J., A. Yamamoto, K. Scearce-Levie, F. Saudou, and R. Hen. 1998. Absence of fenfluramine-induced anorexia and reduced c-Fos induction in the hypothalamus and central amygdaloid complex of serotonin 1B receptor knock-out mice. *J. Neurosci.* 18:5537–5544. https://doi.org/10.1523/jneurosci.18-14-05537.1998

Martin, G.R., A.D. Robertson, S.J. MacLennan, D.J. Prentice, V.J. Barrett, J. Buckingham, A.C. Honey, H. Giles, and S. Moncada. 1997. Receptor specificity and trigemino-vascular inhibitory actions of a novel 5-HT1B/1D receptor partial agonist, 311C90 (zolmitriptan). *Br. J. Pharmacol.* 121:157–164. https://doi.org/10.1038/sj.bjp.0701041

Moran, T.H., and E.E. Ladenheim. 2016. Physiologic and neural controls of eating. *Gastroenterol. Clin. N. Am.* 45:581–599. https://doi.org/10.1016/j.gtc.2016.07.009

Mosienko, V., D. Beis, N. Alenina, and M. Wohr. 2015. Reduced isolation-induced pup ultrasonic communication in mouse pups lacking brain serotonin. *Mol. Autism.* 6:13. https://doi.org/10.1186/s13229-015-0003-6

O'Rahilly, S. 2009. Human genetics illuminates the paths to metabolic disease. *Nature.* 462:307–314. https://doi.org/10.1038/nature08532

Parsons, A.A., R. Valocik, P. Koster, P. Raval, R. Gagnon, N. Tilford, and G. Feuerstein. 1998. Effects of the novel antimigraine agent, frovatriptan, on coronary and cardiac function in dogs. *J. Cardiovasc. Pharmacol.* 32:995–1000. https://doi.org/10.1097/00005344-199812000-00018

Pelosi, B., M. Pratelli, S. Migliarini, G. Pacini, and M. Pasqualetti. 2015. Generation of a Tph2 conditional knockout mouse line for time- and tissue-specific depletion of brain serotonin. *PLoS One.* 10:e0136422. https://doi.org/10.1371/journal.pone.0136422

Poly, T.N., M.M. Islam, H.C. Yang, M.C. Lin, W.S. Jian, M.H. Hsu, and Y.C. Jack Li. 2021. Obesity and mortality among patients diagnosed with COVID-19: A systematic review and meta-analysis. *Front. Med.* 8:620044. https://doi.org/10.3389/fmed.2021.620044

Robbins, L. 2004. Frequent triptan use: Observations on safety issues. *Headache.* 44:178–182. https://doi.org/10.1111/j.1526-4610.2004.04037.x

Roth, B.L. 2016. DREADDs for Neuroscientists. *Neuron.* 89:683–694. https://doi.org/10.1016/j.neuron.2016.01.040

Salvatierra, J., D.A. Lee, C. Zibetti, M. Duran-Moreno, S. Yoo, E.A. Newman, H. Wang, J.L. Bedont, J. de Melo, A.L. Miranda-Angulo, et al. 2014. The LIM homeodomain factor Lhx2 is required for hypothalamic tanycyte specification and differentiation. *J. Neurosci.* 34:16809–16820. https://doi.org/10.1523/JNEUROSCI.1711-14.2014

Saracheva, K., P. Hrischev, L. Vasileva, M. Topolov, J. Nikolova, and D. Getova. 2020. Effects of new generation triptans—frovatriptan and almotriptan—on hemodynamic parameters in intact male and female rats. *Acta Pharm.* 70:239–247. https://doi.org/10.2478/acph-2020-0005

Saudou, F., D.A. Amara, A. Dierich, M. LeMeur, S. Ramboz, L. Segu, M.C. Buhot, and R. Hen. 1994. Enhanced aggressive behavior in mice lacking 5-HT1B receptor. *Science.* 265:1875–1878. https://doi.org/10.1126/science.8091214

Savelieva, K.V., S. Zhao, V.M. Pogorelov, I. Rajan, Q. Yang, E. Cullinan, and T.H. Lanthorn. 2008. Genetic disruption of both tryptophan hydroxylase genes dramatically reduces serotonin and affects behavior in models sensitive to antidepressants. *PLoS One.* 3:e3301. https://doi.org/10.1371/journal.pone.0003301

Scott, M.M., C.J. Wylie, J.K. Lerch, R. Murphy, K. Lobur, S. Herlitze, W. Jiang, R.A. Conlon, B.W. Strowbridge, and E.S. Deneris. 2005. A genetic approach to access serotonin neurons for in vivo and in vitro studies. *Proc. Natl. Acad. Sci. USA.* 102:16472–16477. https://doi.org/10.1073/pnas.0504510102

Sharretts, J., O. Galescu, S. Gomatam, E. Andraca-Carrera, C. Hampp, and L. Yanoff. 2020. Cancer risk associated with lorcaserin: The FDA's review of the CAMELLIA-TIMI 61 trial. *N. Engl. J. Med.* 383:1000–1002. https://doi.org/10.1056/NEJMp2003873

Shimshek, D.R., J. Kim, M.R. Hubner, D.J. Spergel, F. Buchholz, E. Casanova, A.F. Stewart, P.H. Seeburg, and R. Sprengel. 2002. Codon-improved Cre recombinase (iCre) expression in the mouse. *Genesis.* 32:19–26. https://doi.org/10.1002/gene.10023

Simansky, K.J., and D.M. Nicklous. 2002. Parabrachial infusion of D-fenfluramine reduces food intake. Blockade by the 5-HT(1B) antagonist SB-216641. *Pharmacol. Biochem. Behav.* 71:681–690. https://doi.org/10.1016/s0091-3057(01)00740-7

Sohn, J.W., Y. Oh, K.W. Kim, S. Lee, K.W. Williams, and J.K. Elmquist. 2016. Leptin and insulin engage specific PI3K subunits in hypothalamic SF1 neurons. *Mol. Metabol.* 5:669–679. https://doi.org/10.1016/j.molmet.2016.06.004

Sohn, J.W., Y. Xu, J.E. Jones, K. Wickman, K.W. Williams, and J.K. Elmquist. 2011. Serotonin 2C receptor activates a distinct population of arcuate pro-opiomelanocortin neurons via TRPC channels. *Neuron.* 71:488–497. https://doi.org/10.1016/j.neuron.2011.06.012

Stamford, J.A., C. Davidson, D.P. McLaughlin, and S.E. Hopwood. 2000. Control of dorsal raphe 5-HT function by multiple 5-HT(1) autoreceptors: Parallel purposes or pointless plurality?. *Trends Neurosci.* 23:459–465. https://doi.org/10.1016/s0166-2236(00)01631-3

Stoeckius, M., S. Zheng, B. Houck-Loomis, S. Hao, B.Z. Yeung, W.M. Mauck 3rd, P. Smibert, and R. Satija. 2018. Cell Hashing with barcoded antibodies enables multiplexing and doublet detection for single cell genomics. *Genome Biol.* 19:224. https://doi.org/10.1186/s13059-018-1603-1

Tang, X., X. Liu, G. Tao, M. Qin, G. Yin, J. Suo, and X. Suo. 2016. "Self-cleaving" 2A peptide from porcine teschovirus-1 mediates cleavage of dual fluorescent proteins in transgenic Eimeria tenella. *Vet. Res.* 47:68. https://doi.org/10.1186/s13567-016-0351-z

Tecott, L.H., L.M. Sun, S.F. Akana, A.M. Strack, D.H. Lowenstein, M.F. Dallman, and D. Julius. 1995. Eating disorder and epilepsy in mice lacking 5-HT2c serotonin receptors. *Nature.* 374:542–546. https://doi.org/10.1038/374542a0

Thompson, K.J., E. Khajehali, S.J. Bradley, J.S. Navarrete, X.P. Huang, S. Slocum, J. Jin, J. Liu, Y. Xiong, R.H.J. Olsen, et al. 2018. DREADD agonist 21 is an effective agonist for muscarinic-based DREADDs in vitro and in vivo. *ACS Pharmacol. Transl. Sci.* 1:61–72. https://doi.org/10.1021/acsptsci.8b00012

Tong, Q., C.P. Ye, J.E. Jones, J.K. Elmquist, and B.B. Lowell. 2008. Synaptic release of GABA by AgRP neurons is required for normal regulation of energy balance. *Nat. Neurosci.* 11:998–1000. https://doi.org/10.1038/nn.2167

Tullo, V., G. Bussone, S. Omboni, P. Barbanti, P. Cortelli, M. Curone, C. Peccarisi, C. Benedetto, D. Pezzola, D. Zava, and G. Allais. 2013. Efficacy of frovatriptan and other triptans in the treatment of acute migraine of hypertensive and normotensive subjects: A review of randomized studies. *Neurol. Sci.* 34:S87–S91. https://doi.org/10.1007/s10072-013-1367-z

Vanmolkot, F.H., and J.N. de Hoon. 2006. Acute effects of sumatriptan on aortic blood pressure, stiffness, and pressure waveform. *Clin. Pharmacol. Ther.* 80:85–94. https://doi.org/10.1016/j.clpt.2006.03.011

Wang, C., Y. Jiang, J. Ma, H. Wu, D. Wacker, V. Katritch, G.W. Han, W. Liu, X.P. Huang, E. Vardy, et al. 2013. Structural basis for molecular recognition at serotonin receptors. *Science.* 139:610–614. https://doi.org/10.1126/science.1232807

Wang, Q., C. Liu, A. Uchida, J.C. Chuang, A. Walker, T. Liu, S. Osborne-Lawrence, B.L. Mason, C. Mosher, E.D. Berglund, et al. 2014. Arcuate AgRP neurons mediate orexigenic and glucoregulatory actions of ghrelin. *Mol. Metabol.* 3:64–72. https://doi.org/10.1016/j.molmet.2013.10.001

Wyler, S.C., C.C. Lord, S. Lee, J.K. Elmquist, and C. Liu. 2017. Serotonergic control of metabolic homeostasis. *Front. Cell Neurosci.* 11:277. https://doi.org/10.3389/fncel.2017.00277

Xu, J., C.L. Bartolome, C.S. Low, X. Yi, C.H. Chien, P. Wang, and D. Kong. 2018. Genetic identification of leptin neural circuits in energy and glucose homeostases. *Nature.* 556:505–509. https://doi.org/10.1038/s41586-018-0049-7

Xu, Y., J.E. Jones, D. Kohno, K.W. Williams, C.E. Lee, M.J. Choi, J.G. Anderson, L.K. Heisler, J.M. Zigman, B.B. Lowell, and J.K. Elmquist. 2008. 5-HT2CRs expressed by pro-opiomelanocortin neurons regulate energy homeostasis. *Neuron.* 60:582–589. https://doi.org/10.1016/j.neuron.2008.09.033

Xu, Y., J.E. Jones, D.A. Lauzon, J.G. Anderson, N. Balthasar, L.K. Heisler, A.R. Zinn, B.B. Lowell, and J.K. Elmquist. 2010. A serotonin and melanocortin circuit mediates D-fenfluramine anorexia. *J. Neurosci.* 30:14630–14634. https://doi.org/10.1523/JNEUROSCI.5412-09.2010

Yoo, E.S., L. Li, L. Jia, C.C. Lord, C.E. Lee, S.G. Birnbaum, C.R. Vianna, E.D. Berglund, K.A. Cunningham, Y. Xu, et al. 2021. Galphai/o-coupled Htr2c in the paraventricular nucleus of the hypothalamus antagonizes the anorectic effect of serotonin agents. *Cell Rep.* 37:109997. https://doi.org/10.1016/j.celrep.2021.109997

Yu, H., M. Rubinstein, and M.J. Low. 2021. Developmental single-cell transcriptomics of hypothalamic POMC progenitors reveal the genetic trajectories of multiple neuropeptidergic phenotypes. *bioRxiv*. https://doi.org/10.1101/2021.05.12.443898

Supplemental material

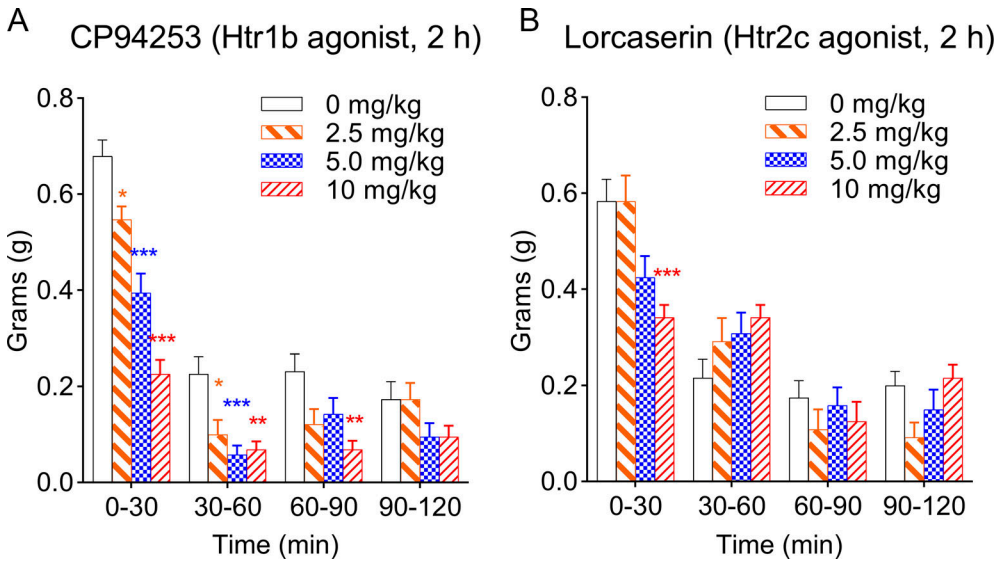

Figure S1. **The anorexigenic effect of CP94235 and lorcaserin in a fast-refeeding test. (A)** 2-h refeeding in C57BL/6 mice that received either vehicle or CP94253 after an overnight (18 h) fast. Food intake data were binned into 30-min intervals. n = 19, F (9, 216) = 6.573, P < 0.001. **(B)** 2-h refeeding in C57BL/6 mice that received either vehicle or lorcaserin after an overnight fast. Food intake data were binned into 30-min intervals. n = 12, F (9, 130) = 4.528, P < 0.001. Two-way ANOVA with Dunnett's post hoc tests. In each 30-min interval, food intake in drug-treated mice was compared to that in vehicle-treated mice. *, P < 0.05; **, P < 0.01; and ***, P < 0.001. All data were verified in at least two independent experiments.

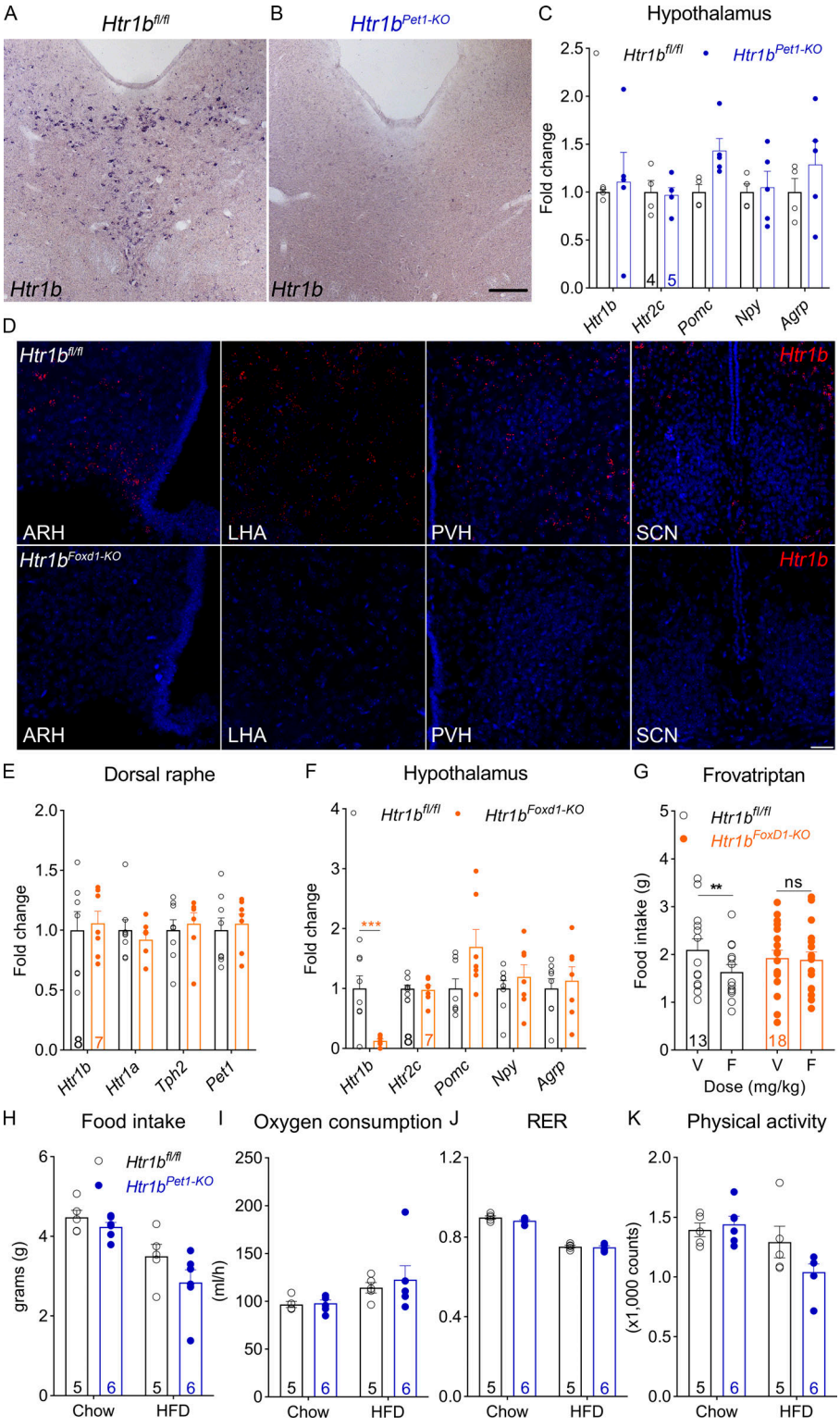

Figure S2. **Validation of the deletion of *Htr1b* in *Htr1b*$^{Pet1\text{-}KO}$ and *Htr1b*$^{Foxd1\text{-}KO}$ mice. (A and B)** Digoxigenin in situ hybridization against *Htr1b* mRNA in the dorsal raphe of *Htr1b*$^{fl/fl}$ (A) and *Htr1b*$^{Pet1\text{-}KO}$ (B) mice. Scale bar is 100 µm. **(C)** qPCR analyses of mRNA expression in the hypothalamus of *Htr1b*$^{fl/fl}$ and *Htr1b*$^{Pet1\text{-}KO}$ mice. **(D)** In situ hybridization of *Htr1b* mRNA (red, RNAscope) in the hypothalamus of *Htr1b*$^{fl/fl}$ and *Htr1b*$^{Foxd1\text{-}KO}$ mice. Scale bar is 20 µm. **(E and F)** qPCR analyses of mRNA expression in the dorsal raphe (E) and hypothalamus (F) of *Htr1b*$^{fl/fl}$ and *Htr1b*$^{Foxd1\text{-}KO}$ mice. **(G)** The anorectic effect of frovatriptan in *Htr1b*$^{fl/fl}$ and *Htr1b*$^{Foxd1\text{-}KO}$ mice, n = 13–18, $F(1, 29) = 4.71$, $P = 0.038$. **(H)** Daily food intake in *Htr1b*$^{fl/fl}$ and *Htr1b*$^{Pet1\text{-}KO}$ mice fed a chow diet or HFD, $F(1, 9) = 0.785$, $P = 0.4$. **(I)** Oxygen consumption in *Htr1b*$^{fl/fl}$ and *Htr1b*$^{Pet1\text{-}KO}$ mice fed a chow diet or HFD, $F(1, 9) = 0.136$, $P = 0.72$. **(J)** Respiratory exchange ratio (RER) in *Htr1b*$^{fl/fl}$ and *Htr1b*$^{Pet1\text{-}KO}$ mice fed a chow diet or HFD, $F(1, 9) = 0.82$, $P = 0.39$. **(K)** Physical activity in *Htr1b*$^{fl/fl}$ and *Htr1b*$^{Pet1\text{-}KO}$ mice fed a chow diet or HFD, $F(1, 9) = 1.028$, $P = 0.33$. Data are presented as mean ± SEM. Unpaired t test in C, E, and F. Two-way ANOVA with Sidak's post hoc tests in G, H, I, J, and K. **, $P < 0.01$; ***, $P < 0.001$. All data were verified in at least two independent experiments.

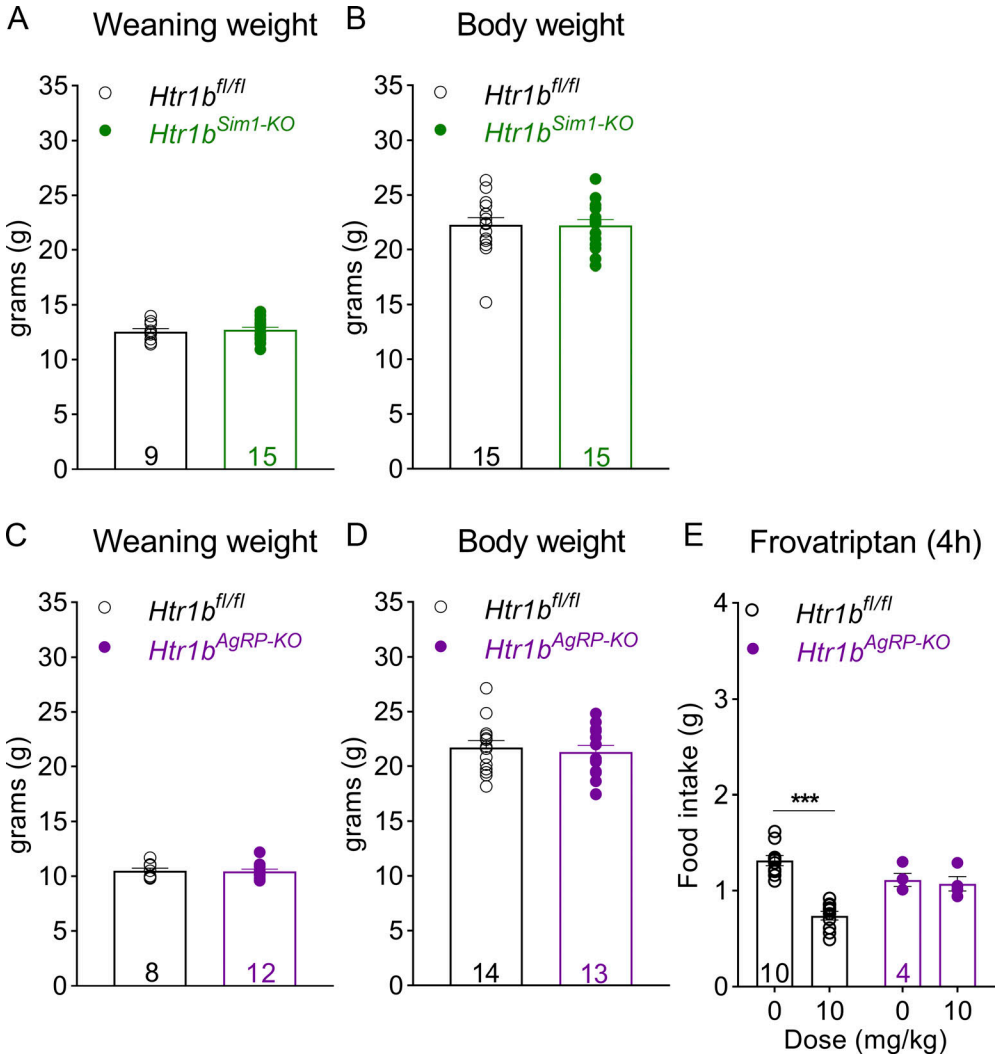

Figure S3. **Normal body weight in *Htr1b*$^{Sim1\text{-}KO}$ and *Htr1b*$^{Agrp\text{-}KO}$ mice. (A)** Body weight at 3 wk of age, n = 9–15, P = 0.7. **(B)** Body weight at 8 wk of age, n = 15, P = 0.96. **(C)** Body weight at 3 wk of age, n = 8–12, P = 0.92. **(D)** Body weight at 8 wk of age, n = 13–14, P = 0.66. Data are presented as mean ± SEM. **(E)** The anorectic effect of frovatriptan in *Htr1b*$^{fl/fl}$ and *Htr1b*$^{Agrp\text{-}KO}$ mice, n = 4–10, $F(1, 12) = 34.97$, $P < 0.001$. Unpaired t test in A–D. Two-way ANOVA with Sidak's post hoc tests in E, ***, $P < 0.001$. All data were verified in at least two independent experiments.

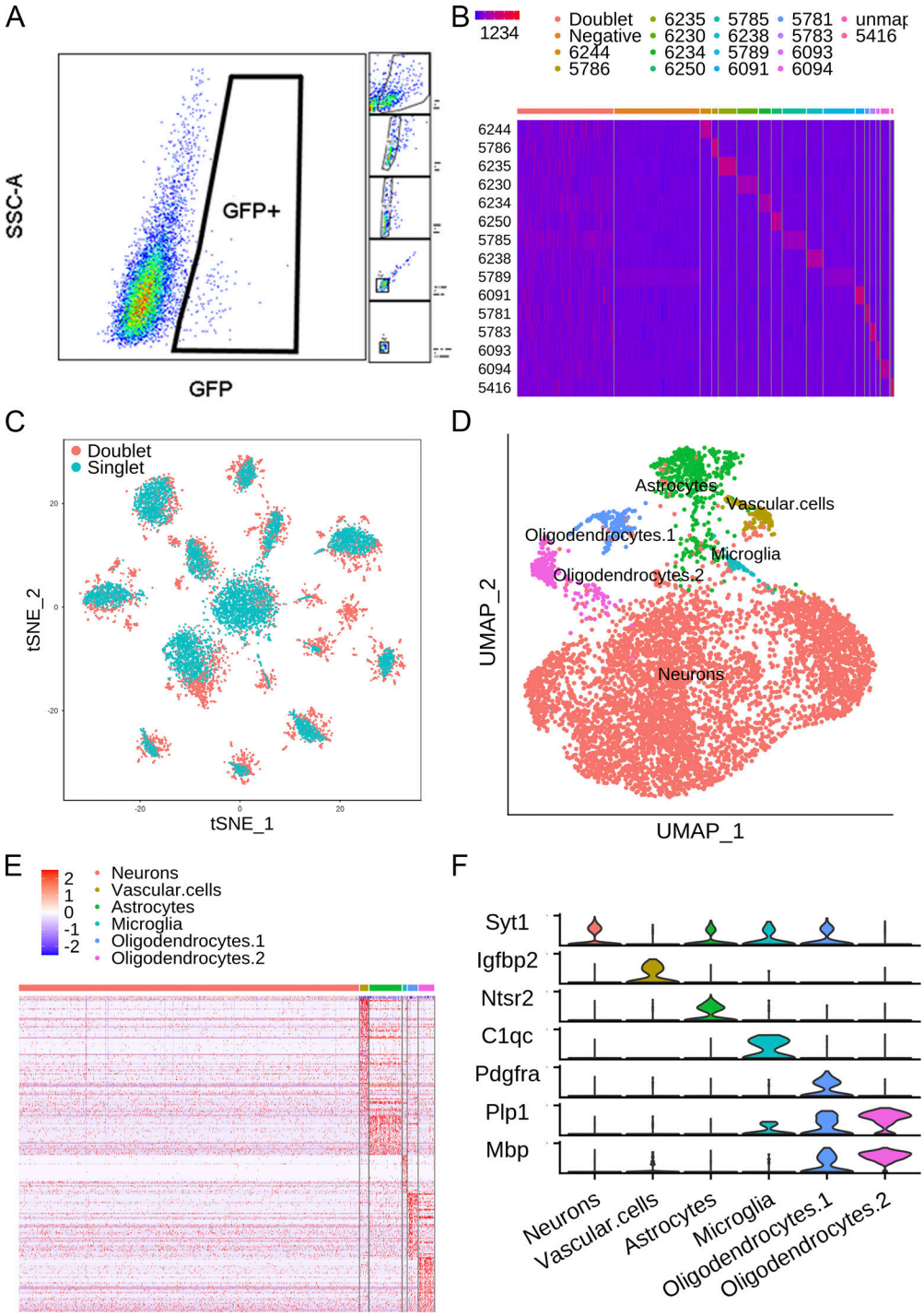

Figure S4. **snRNA-seq analyses of ARH neurons in the adult AgRP-Cre; Sun1-GFP mice. (A)** Flow cytometry sorting GFP positive nuclei from 15 adult AgRP-Cre; Sun1-GFP mice. **(B)** Heatmap of normalized HTO values based on HTOdemux. Doublets (or multiplets) express more than one HTO signature. **(C)** tSNE embedding of the HTO dataset revealed 15 singlet clusters. **(D)** Transcriptome-based dimensionality reduction using UMAP identified neuronal and non-neuronal clusters. **(E)** Heatmap of the marker genes for the six identified clusters in the UMAP aggregate of all cells. **(F)** Violin plot of the key marker genes in the six identified clusters.

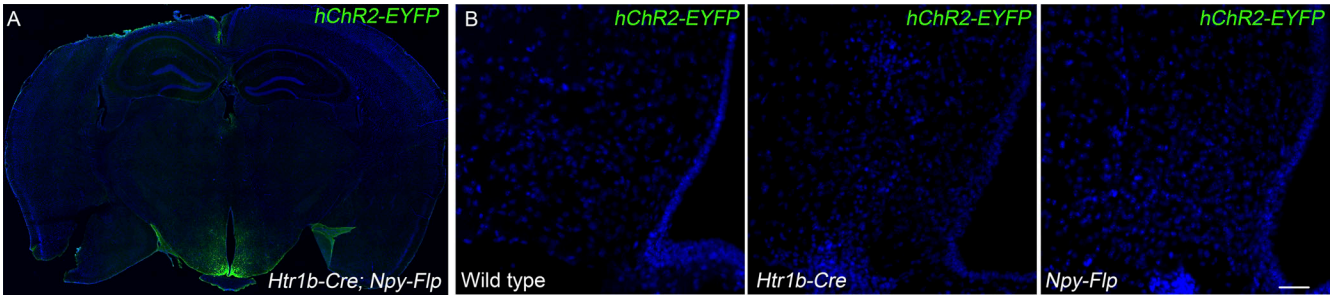

Figure S5. **Validation of Cre- and Flp-dependent hChR2-EYFP expression. (A)** Low magnification image showing the specific labeling of the ARH *Htr1b-Cre/Npy-Flp* expressing neurons in the hypothalamus. **(B)** No leakage of hChR2-EYFP expression in the ARH of wild-type (left), $Htr1b^{Cre/+}$ (middle), or $Npy^{Flp/+}$ (right) mice after stereotaxic injections of the Cre- and Flp-dependent constructs. Scale bars are 20 µm. All data were verified in at least two independent experiments.